

1 **Marine eukaryote community responses to the climate and oceanographic changes in**
2 **Storfjordrenna (southern Svalbard) over the past ~13.3 kyr BP: Insights from sedimentary**
3 **ancient DNA analysis**

4 Hasitha Nethupul^{1*}, Magdalena Łacka¹, Marek Zajączkowski¹, Dhanushka Devendra¹, Ngoc-Loi
5 Nguyen¹, Jan Pawłowski¹, Joanna Pawłowska¹

6 ¹Department of Palaeoceanography, Institute of Oceanology, Polish Academy of Sciences, Sopot
7 81-712, Poland

8 * *Correspondence to:* Hasitha Nethupul (nethupul@iopan.pl)

9

10 **Abstract**

11 Sedimentary ancient DNA (sedaDNA) metabarcoding is an emerging method for reconstructing
12 the responses of marine organisms to past climate and oceanographic changes, including rare and
13 non-fossilized taxa. Marine *sedaDNA* records from the Arctic are scarce, especially those focusing
14 on the impact of environmental shifts on the biodiversity and functional composition of marine
15 eukaryote communities. Here, we present a *sedaDNA* eukaryotic record from a sediment core
16 retrieved in Storfjordrenna, southern Svalbard, spanning the termination of the Bølling-Allerød,
17 the Younger Dryas, and the Holocene (13.3 - 1.3 kyr BP). We successfully recovered the eukaryotic
18 communities and identified them by their ecological roles. Our study showed that the eukaryotic
19 biodiversity in Storfjordrenna remained relatively stable, except during transitions between major
20 climatic intervals. These shifts were characterized by changes in richness and relative abundance,
21 driven by factors such as perennial ice cover, surface water cooling, and subsurface Atlantic water
22 influx. Cercozoans and Marine Stramenopiles (MAST) emerged as dominant heterotrophs,
23 characterized by high ecological flexibility and broad tolerance. Primary productivity was
24 primarily driven by Arctic water (ArW) associated phytoplankton, including diatoms
25 (*Thalassiosira* and *Chaetoceros*), green algae (*Micromonas*), and autotrophic dinoflagellates
26 (*Polarella glacialis*), as well as the mixoplanktonic silicoflagellate *Pseudopedinella elastica*.
27 Amplicon sequence variant (ASV)-based indicator analysis revealed that uncultured cercozoan
28 lineages and MAST taxa were primarily associated with Atlantic water (AW) proxies, whereas
29 parasitic dinoflagellates (Dino-group I) and choanoflagellates were more closely aligned with ArW
30 proxies. Analysis of indicator responses shows the complex interactions within eukaryotic
31 communities, and reveals a strong association among functional ecological groups that impact
32 ecosystem productivity and regulation. This complexity highlights the limitations of traditional
33 single-proxy approaches to accurately reconstructing paleoenvironmental conditions. Our study
34 demonstrates the potential of high-resolution marine *sedaDNA* metabarcoding in elucidating
35 responses to past climate changes, improving our understanding of the intricate interactions within
36 eukaryotic communities, and enhancing our knowledge of marine ecosystems.

37

38 **1. Introduction**

39 The Arctic marine ecosystem is undergoing rapid and profound changes, primarily driven by
40 climate warming (IPCC, 2023; Polyakov et al., 2017; Polyakov et al., 2020). A prominent feature
41 of these changes is the increased influx of AW into the region, a phenomenon known as
42 Atlantification. This process is associated with warming and rise of sea surface temperatures
43 (SST), reduced sea-ice cover, altered salinity patterns, and changes in nutrient dynamics (Årthun
44 et al., 2012; Polyakov et al., 2017).

45 These transformations in the marine environment are altering the biodiversity of the Arctic
46 region and impacting the function and resilience of its ecosystems (Benner et al., 2019;
47 Hallegraeff, 2010; Ribeiro et al., 2024). The Storfjordrenna region in southern Svalbard is an ideal
48 location to study these shifts, having experienced significant climate-driven changes over the last
49 ~14,000 years, driven by meltwater discharge and the interaction between cold ArW and warmer
50 AW inflows (Łącka et al., 2019; Łącka et al., 2015; Pawłowska et al., 2020; Telesiński et al., 2024).
51 The region's biodiversity has been shaped by, and remains sensitive to, these fluctuating and
52 dynamic environmental conditions (Bensi et al., 2024; Deb and Bailey, 2023; Górska et al., 2022;
53 Hop et al., 2019). Understanding how biodiversity adapts to such changes is essential for
54 reconstructing past ecological responses to climate change and for predicting future trends.
55 Although the impact of climate change on Arctic marine ecosystems is well documented (Deb and
56 Bailey, 2023; Wassmann et al., 2010), relatively few studies have examined marine ecosystems
57 using sedaDNA to analyze long-term biodiversity patterns (Grant et al., 2024; Pawłowska et al.,
58 2020; Zimmermann et al., 2023). Recent developments in sedaDNA techniques have increased our
59 ability to extract and analyze DNA from marine environments, providing valuable insights into
60 eukaryotic communities and their responses to environmental changes over geological time scales
61 (Grant et al., 2024; Harðardóttir et al., 2024; Zimmermann et al., 2021). Moreover, several studies
62 have suggested that the sedaDNA or environmental DNA (eDNA) approach has the potential to
63 use specific ASVs as proxies/bioindicators, even when their taxonomy is unknown thereby
64 strengthening the connection between ASVs and ecological functions and environmental changes
65 (Grant et al., 2024; Harðardóttir et al., 2024; Li et al., 2023; Lin et al., 2022; Pawłowska et al.,
66 2020; Perret-Gentil et al., 2021; Perret-Gentil et al., 2017; Zimmermann et al., 2021). Studies of
67 marine eukaryotic sedaDNA have demonstrated that even low-resolution records can provide
68 significant data on the shifts in marine communities over time, offering insight into past ecosystem

69 dynamics (Grant et al., 2024). For example, recent studies have demonstrated that the sedaDNA
70 approach can be used to reconstruct interactions between sea ice cover, ocean temperatures, and
71 eukaryotic community composition (Armbrecht, 2020; Grant et al., 2024; Harðardóttir et al., 2024;
72 Zimmermann et al., 2023; Zimmermann et al., 2021). However, there is still a significant lack of
73 suitable-resolution marine eukaryotic sedaDNA records from the Arctic, especially those focusing
74 on the, ecosystem-oriented approaches that integrate ecological roles and biotic interactions to
75 better link past biodiversity changes with ecosystem functioning and environmental changes.

76 This study addresses this issue by reconstructing the long-term history of marine eukaryotic
77 communities from Storfjordrenna, southern Svalbard, using sedaDNA metabarcoding using V1V2
78 primers that capture both planktonic and benthic taxa with adequate taxonomic resolution for
79 ecological interpretation (Fonseca et al., 2010; Lindeque et al., 2013; Sinniger et al., 2016). . The
80 sedaDNA record is supported by previously published sedimentological, micropaleontological,
81 and geochemical records (Łącka et al., 2019; Łącka et al., 2020; Łącka et al., 2015; Telesiński et
82 al., 2024). By focusing on eukaryotic communities associated with ArW and AW masses, we aim
83 to assess their structure, ecological roles, and potential as indicators of past environmental
84 conditions. Our approach seeks to identify how marine ecosystem have responded to significant
85 climate-driven changes in this region and how these responses can improve our understanding of
86 the future trajectories of Arctic marine biodiversity in the context of ongoing climate warming.

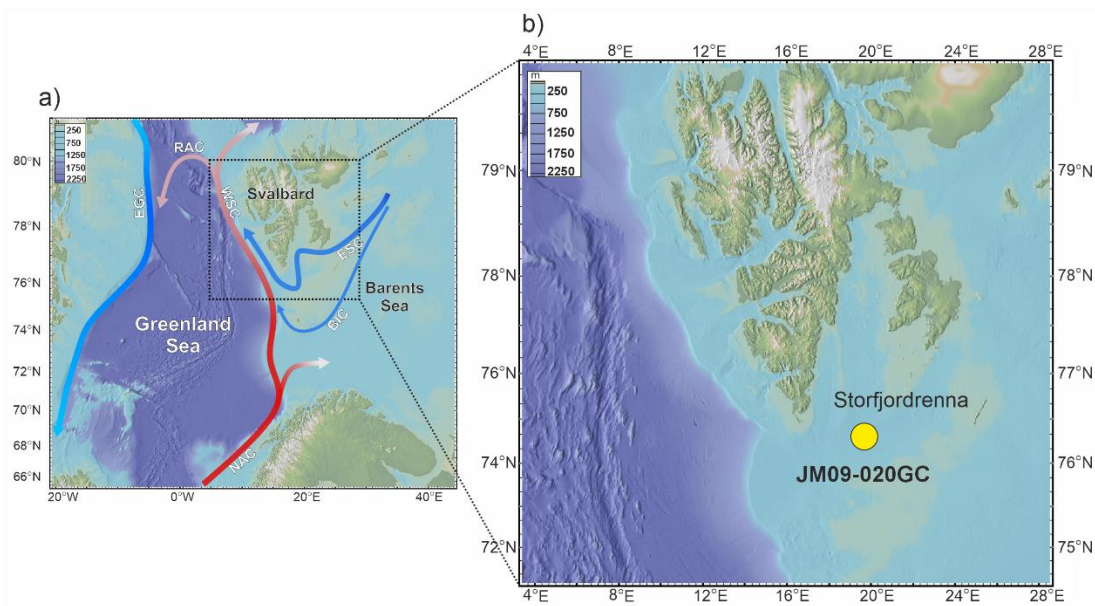
87

88 **2. Study area**

89 Storfjorden is an open fjord system located in the Svalbard archipelago, between the islands of
90 Spitsbergen, Barentsøya, and Edgeøya (**Fig. 1a**). The cross-shelf through Storfjordrenna is located
91 south of Storfjorden's mouth. The hydrography of Storfjorden and Storfjordrenna is primarily
92 governed by the interplay of two major water masses: AW and ArW. AW is characterized by
93 relatively high temperatures ($>3\text{ }^{\circ}\text{C}$) and high salinity ($>34.95\text{ PSU}$), whereas ArW exhibits lower
94 temperatures ($<0.5\text{ }^{\circ}\text{C}$) and salinity ranging from 34.3 PSU to 34.8 PSU (Bensi et al., 2024;
95 Skogseth et al., 2020; Sundfjord et al., 2017). AW is transported northwards by the Norwegian
96 Atlantic Current, which bifurcates upon entering the Barents Sea into the West Spitsbergen Current
97 and the North Cape Current (Blindheim and Østerhus, 2005). In contrast, ArW enters the region
98 via the East Spitsbergen Current and the Bear Island Current, bringing cold, less saline waters into

99 the Barents Sea (Hopkins, 1991). AW enters Storfjordrenna in a cyclonic manner, following the
100 bathymetry. The Polar Front, which separates AW and ArW water masses, is located along the
101 slope of Storfjordrenna (Bensi et al., 2024). The biological and geochemical signals preserved in
102 the sediments represent an integrated response to both gradual and abrupt climatic and
103 oceanographic changes (Łącka et al., 2019; Łącka et al., 2015). Therefore, the site's proximity to
104 the Arctic Front facilitates the detection of subtle ecosystem responses to long-term warming and
105 changing oceanographic regimes.

106



107

108 **Figure 1.** a) Map of the study area and (b) location of core JM09-020GC (yellow dot). Red arrows
109 indicate warm currents, and blue arrows indicate cold currents. Abbreviations: NAC: North
110 Atlantic Current, WSC: West Spitsbergen Current, RAC: Return Atlantic Current, ESC: East
111 Spitsbergen Current, BIC: Bear Island Current, EGC: East Greenland Current.)

112 3. Materials and Methods

113 3.1 Sediment core and age model

114 Gravity core JM09-020-GC was collected in 2009 at a depth of 253 m in Storfjordrenna,
115 northwestern Barents Sea during the expedition of R/V Jan Mayen (**Fig. 1b**). The core was stored
116 and processed according to the methods described by (Łącka et al., 2019; Łącka et al., 2020; Łącka

117 et al., 2015). The chronology of the core was established based on AMS¹⁴C radiocarbon dating and
118 one additional tie point defined by the appearance of vivianite micro-concretions in a sediment
119 layer set to 12.8 kyr BP, coinciding with the onset of the Younger Dryas (**Table S1**)(Łącka et al.,
120 2020). The dates published first by Łącka et al.(2015), and Łącka et al. (2020) were recalibrated
121 using the Marine20 calibration curve (**Fig. S1, Table S1**)(Heaton et al., 2020). The
122 palaeoceanographic history of Storfjordrenna over the past ~14,000 years is well documented
123 through detailed, multi-proxy reconstructions. These include analyses of fossil foraminifera
124 assemblages, isotopic composition of foraminiferal tests, grainsize and elemental composition of
125 sediments, alkenones (Łącka et al., 2019; Łącka et al., 2015), and dinoflagellate cysts (Telesiński
126 et al., 2024).

127 **3.2 sedaDNA workflow**

128 **3.2.1 DNA extraction, amplification, and sequencing**

129 Approximately 10 g of sediment was collected from 55 sediment layers using sterile spoons
130 and transferred to sterile containers. DNA extractions were performed using the DNeasy
131 PowerMax Soil Kit (Qiagen), following the manufacturer's instructions. All DNA extracts were
132 stored at -20°C until PCR amplification.

133 The V1V2 region of the 18S rDNA (with a length of ~340 bp) was amplified by PCR using the
134 forward primer SSU_FO4mod (5'-GCT TGW CTC AAA GAT TAA GCC-3') and the reverse
135 primer SSU_R22 (3'-CCT GCT GCC TTC CTT RGA-5') (Fonseca et al., 2010; Lindeque et al.,
136 2013), which were tagged with a unique 8-nucleotide sequence at their 5' ends (Esling et al., 2015).
137 We followed the protocols established and positively tested by Pawłowska et al. (2020);
138 Pawłowska et al. (2014) and Lejzerowicz et al. (2013), with minor adjustments to the number of
139 PCR cycles based on sample-specific amplification performance. Each sample was amplified in
140 triplicate and each PCR reaction was performed in a total volume of 25 µL, which included 1.5 µL
141 of 1.5 mM MgCl₂ (Applied Biosystems, USA), 2.5 µL of 10× PCR buffer II (Applied Biosystems),
142 0.5 µL of 0.2 mM deoxynucleotide triphosphates (Promega, USA), 0.5 µL of 20 mg/ mL bovine
143 serum albumin (Invitrogen Ultrapure, USA), 1 µL of 10 µM of each primer, 0.2 µL of AmpliTaq
144 Gold DNA polymerase (Applied Biosystems) and 2 µL of template DNA. The amplification
145 conditions consisted of a pre-denaturation step at 95°C for 5 min, followed by 50 cycles of
146 denaturation at 95°C for 30 s, annealing at 57°C for 30 s and extension at 72°C for 1 min, followed

147 by a final extension step at 72°C for 5 min. PCR products, including negative control for each
148 unique combination of tag-encoded primers, were verified by agarose gel electrophoresis. PCR
149 products were purified using the High Pure PCR Cleanup Micro Kit (Roche) and quantified using
150 a Qubit 2.0 fluorometer. Libraries were pooled in equimolar quantities and the sequence library
151 was prepared using a TruSeq library-preparation kit (Illumina). Samples were then loaded into a
152 MiSeq instrument for a paired-end run of 2*250 cycles. The sequencing was performed at the
153 University of Geneva.

154 **3.2.2 Data quality control and processing**

155 The raw sequencing reads for each sample were processed using the SLIM web application
156 (Dufresne et al., 2019). In brief, the module *demultiplexer* was used to demultiplex the raw reads
157 according to their unique tags in the forward and reverse reads. Quality filtering, chimera removal
158 and ASVs table generation were performed using DADA2 v.1.16 with pseudo-pool parameters
159 (Callahan et al., 2015).

160 The ASVs were then curated using the LULU package v.0.1.0 (Froslev et al., 2017) with the
161 default parameters. The taxa assignment of the ASVs was performed using VSEARCH against the
162 taxonomically curated PR2 database v.4.14.1 (Guillou et al., 2012), which contains functional
163 annotations. We used a Last Common Ancestor approach, assigning to the consensual taxonomic
164 rank to up to reference sequences with at least 80% similarity as a threshold for the dataset. The
165 ASVs were also assigned to functional groups with at least 95% similarity; with the functional
166 attributes of Ibarbalz et al. (2019). The ASVs assigned to prokaryotes (bacteria and archaea) were
167 removed in order to analyze only eukaryotic ASVs. Additionally, fungi and gymnamoebae were
168 removed due to the high risk of contamination (Armbrecht, 2020). Unique ASVs (occurring in
169 only one sample), short sequences (<200 bp), rare ASVs (having <100 reads), and low read count
170 samples (< 1000 reads) were removed from the dataset. Additionally, the unassigned sequences
171 were blasted with NCBI to further clarify the taxonomic composition. The Cumulative Sum
172 Scaling (CSS) technique (scale factor - 0.9) was used to transform the read counts in the dataset
173 and using ‘cssNorm’ function in the genomeSeq package (Paulson et al., 2013), and used for the
174 downstream statistical analysis in the study.

175 3.3 Statistical analysis

176 Data analysis was performed in R v.4.5.2 (Team, 2025) using several R packages. The relative
177 abundances of reads and ASVs for each eukaryote group were calculated and plotted using *ggplot2*
178 (Wickham, 2016) and Grapher 24.1.213.

179 Three alpha diversity indices were calculated for all samples (ASV richness $q = 0$, Shannon
180 index $q = 1$, and Simpson index $q = 2$) based on the functions in the *vegan* package (Oksanen et
181 al., 2025). Shannon diversity was compared between the main groups using the Kruskal-Wallis's
182 rank test in the *stats* package (Kruskal and Wallis, 1952). Significance between the groups was
183 determined using a pairwise Wilcoxon rank sum test with an adjusted p value (Benjamini-
184 Hochberg) in the *ggpubr* package (Kassambara, 2018). A Principal Coordinate Analysis (PCoA)
185 ordination was generated using the Bray-Curtis dissimilarity matrix calculated using the *ape*
186 package (Paradis and Schliep, 2019) and *stringer* package (Wickham, 2025) to assess beta
187 diversity and visualize dissimilarities in eukaryotic community composition among the samples.
188 Permutational Multivariate Analysis of Variance (PERMANOVA) with 999 permutations via the
189 *adonis2* function in the *vegan* package (Oksanen et al., 2025).

190 A co-occurrence heatmap representing most of the families in the study was generated. The
191 *corrplot* and *pheatmap* packages (Kolde, 2025; Wei and Simko, 2024) were used to analyze the
192 correlation between eukaryote families based on spearman method (a cutoff mark in correlation as
193 > 0.5 , and p value Benjamini-Hochberg (BH) adjusted < 0.05). Environmental parameters
194 represented by palaeoceanographic proxies were used to identify the response of eukaryote species
195 using three analytical methods. Seven proxies were used, including indicators of: i) sea surface
196 temperature (SST U_{37}^{K*}) Łącka et al. (2019), ii) AW (foraminifera *Nonionellina labradorica* and
197 *Buccella frigida* Łącka et al. (2015), and dinocyst *Operculodinium centrocarpum* (Telesiński et
198 al., 2024), iii) ArW/meltwater (%C37:4 Łącka et al. (2019), iv) glaciomarine condition
199 (foraminifera *Elphidium excavatum* and *Cassidulina reniforme* Łącka et al. (2015), v) sea ice
200 (dinocyst *Echinidinium karaense* Telesiński et al. (2024), and vi) bottom current dynamics (mean
201 grain size 0-63 μm) Łącka et al. (2015). Multidimensional Fuzzy Set Ordination (MFSO)
202 correlation plot, and Fuzzy set ordination (FSO) plots were generated for each environmental
203 variable to assess their influence on eukaryote communities and identify key proxies for
204 downstream analysis (Roberts, 2008). Firstly, a heatmap of sparse partial least squares (sPLS)
205 regression between ASVs, and proxies was generated using the *spls* and *cim* function in *mixOmics*

206 package (Froslev et al., 2017; Rohart et al., 2017). The potential ASV based indicators were
207 selected based on a correlation coefficient threshold of > 0.3 and BH adjusted p value of < 0.05 .
208 Secondly, a Spearman correlation heatmap of the top 100 most significant ASVs ($\rho > 0.3$ and p-
209 adjust < 0.05) as generated using the *pheatmap* package. Finally, the dataset was analyzed using
210 DEseq2 analysis, and the dataset was curated based on $\log_2\text{FoldC} \geq 1$ (BH-adjusted p value $<$
211 0.05), and lower base mean (Love et al., 2014). Potential indicator ASVs were categorized based
212 on their correlation strength and consistent detection across at least two methods or strong
213 association with multiple paleo-proxies.

214 **4. Results**

215 **4.1 Metabarcoding data**

216 A total of 2,620,808 raw sequence reads were generated from 55 samples. After initial quality
217 filtering and denoising with DADA2 in SLIM, eight samples were excluded due to low number of
218 reads (< 300). An additional five samples were removed during the downstream eukaryote-specific
219 quality control process described in the Methods. This reduced our dataset to 1,609,500 sequence
220 reads and 273 ASVs in 42 samples (**Table S2, S3**).

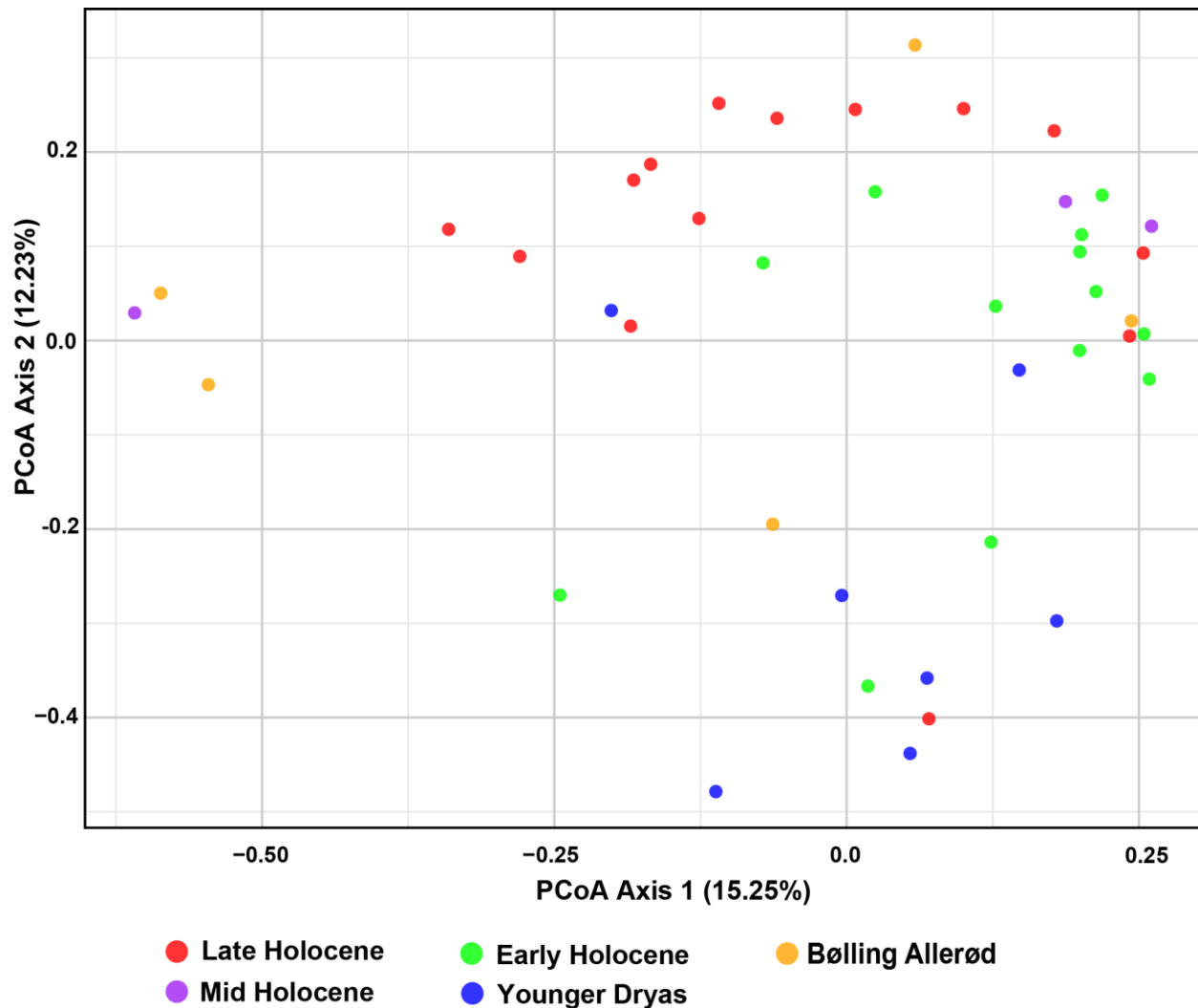
221 **4.2 Alpha diversity**

222 Alpha diversity indices varied across time interval; however, Shannon diversity showed no
223 significant differences among intervals (Kruskal–Wallis, $p = 0.48$; **Fig. S2, Table S2**). This
224 apparent discrepancy reflects that species richness is sensitive to rare taxa, whereas Shannon
225 diversity accounts for both richness and evenness, making it less responsive to occasional low-
226 abundance ASVs. Overall, the number of observed ASVs ranged from 4 to 144 (**Fig. S2, Table**
227 **S2**). The highest values were observed in the Younger Dryas, the Early and Late Holocene,
228 particularly at 12.3 kyr BP, 11.3 kyr BP, 9.5 kyr BP, 4.0 kyr BP, and 2.8-2.3 kyr BP. In contrast,
229 a significant decrease in richness was observed around 13.3 kyr BP, 11.8 kyr BP, 2.17 kyr BP, and
230 1.8 kyr BP (**Fig. S2, Table S2**). Similar trends were revealed by both the Shannon and Simpson
231 indices, with minimal diversity observed around 12.8 kyr, 11.7 kyr, 9.2 kyr, and 3.4 kyr BP.
232 Between 11.7 kyr and 9.2 kyr BP. Due to limited data resolution, no clear trends in alpha diversity
233 could be discerned between 9.2 kyr and 3.4 kyr BP. However, a decline was evident after 3.4 kyr
234 BP, continuing towards 1.3 kyr BP (**Fig. S2**).

235 4.3 Beta Diversity

236 Beta diversity analyses revealed minor changes in community composition during the
237 transitions from the Bølling-Allerød to the Younger Dryas, and from the Younger Dryas to the
238 Holocene (**Fig. 2**). The PCoA plot revealed partial overlap across different time intervals, with
239 Early Holocene and Younger Dryas samples were widely dispersed, while Late Holocene samples
240 clustered separately along Axis 2, respectively. In contrast, Bølling-Allerød and Mid Holocene
241 samples were largely scattered along the Axis 2 (**Fig. 2**). PERMANOVA results confirmed a
242 significant effect of the time intervals on eukaryote community ($R^2 = 0.16$, $p < 0.05$), with
243 significant pairwise differences detected between the Late and Early Holocene, Late Holocene and
244 Younger Dryas, Early Holocene and Younger Dryas, and Younger Dryas and Bølling–Allerød
245 (**Table S4**). FSO plots revealed a significant relationship between the samples and several paleo-
246 environmental proxies, including the dinocyst *Operculodinium centrocarpum* from (Telesiński et
247 al., 2024), ArW/meltwater indicator (%C37:4) (Łącka et al., 2019), and sea surface temperature
248 (SST U_{37}^{K*}) (Łącka et al., 2019) (**Fig. S3**). In the MFSO framework, these proxies together explained
249 a moderate proportion of the variation in community composition (cumulative fuzzy set correlation
250 $r = 0.454$). (**Fig. S3**).

251



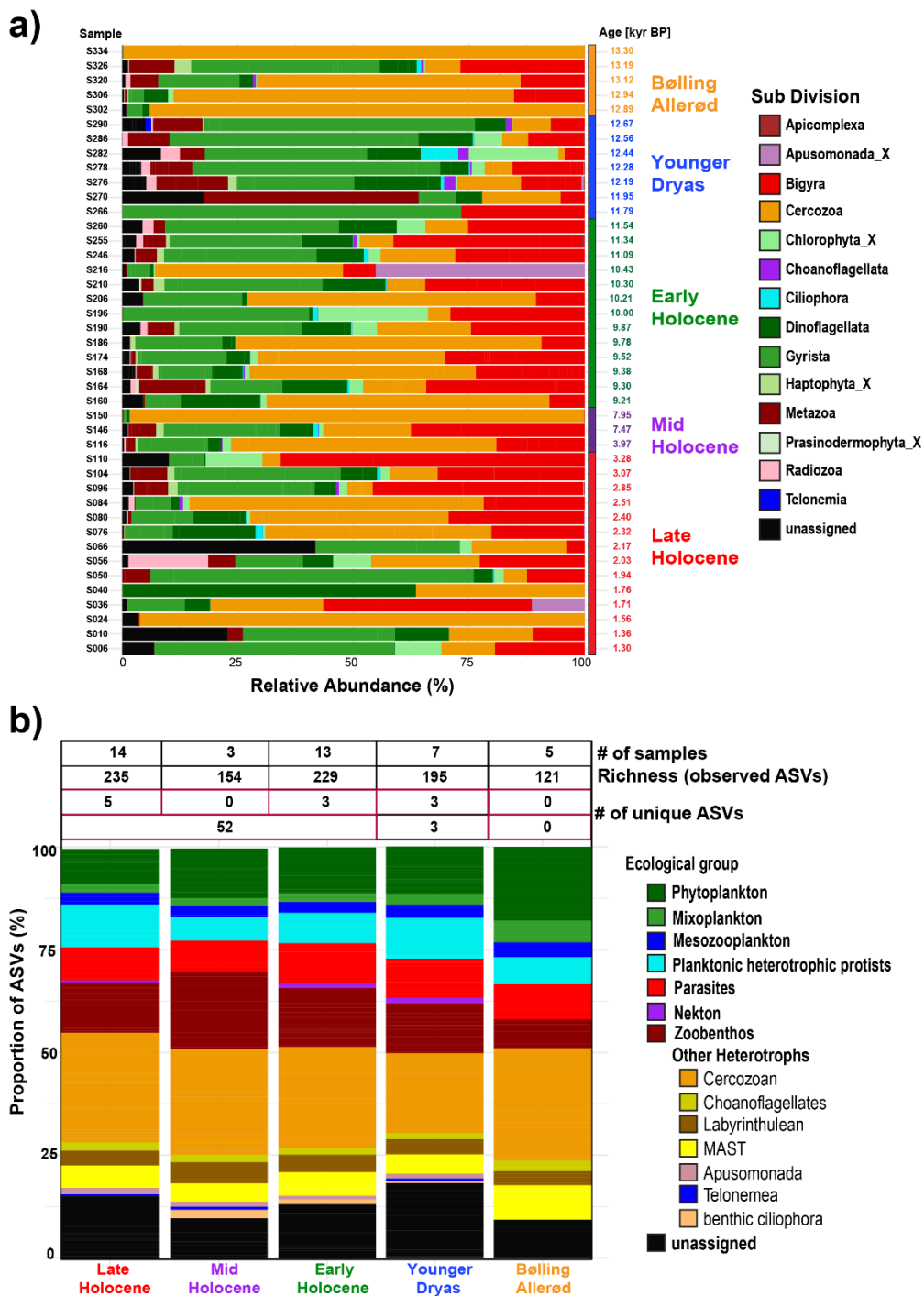
252

253 **Figure 2.** PCoA based on the Bray-Curtis dissimilarity matrix method with the eukaryote dataset
 254 (raw data converted into CSS formation).

255 4.4 Community composition

256 Within the dataset, a total of 236 ASVs were assigned to 14 Sub-Divisions, while 37 ASVs
 257 remained unassigned (**Table S3**). The Cercozoa was the most abundant sub-division, comprising
 258 67 ASVs, accounting for 24.54% of the total ASVs (**Fig. 3, Table S3**). Overall, the taxonomic
 259 structure of eukaryotes based on read abundance fluctuated significantly between samples (**Fig.**
 260 **3a**). In contrast, ASV richness remained stable across different time periods except during the
 261 Bølling-Allerød period (**Fig.3b**). The number of unique ASVs was highest during the Late
 262 Holocene, with five unique ASVs identified. The Younger Dryas and Early Holocene each
 263 exhibited three unique ASVs. Conversely, no distinctive ASVs were identified during the Mid

264 Holocene and Bølling–Allerød periods. Across the entire Holocene, a total of 52 unique ASVs
 265 were recorded (Fig.3b).



266
 267 **Figure 3:** (a) Bar plot showing the downcore distribution of eukaryotic sub-divisions based on
 268 their relative abundance. (b) Proportional richness of distinct ecological groups across selected
 269 time periods (Bølling-Allerød, Younger Dryas, Early Holocene, Mid Holocene, and Late

270 Holocene), expressed as the percentage of ASVs. The accompanying table provides the number of
271 samples, the total number of observed ASVs and unique ASVs within each climate time interval.

272
273 The ASVs were categorized based on their ecological roles, such as phytoplankton (31 ASVs),
274 mixoplankton (7 ASVs), mesozooplankton (8 ASVs), planktonic heterotrophic protists (23 ASVs),
275 parasites (24 ASVs), zoobenthos (36 ASVs), nekton (2 ASVs), and other heterotrophs (104 ASVs)
276 (**Fig. 3b, Table S3**). The latter category comprises multiple taxonomic groups characterized by
277 complex habitats and feeding behaviors, many of which have poorly understood ecological roles.
278 This group includes Cercozoa (67 ASVs), Labyrinthulea (11 ASVs), Choanoflagellata (5 ASVs),
279 MAST (15 ASVs), benthic ciliophora (2 ASVs), Apusomonada (3 ASVs), and one ASV from the
280 Telonemea flagellate group. The unassigned taxa (37 ASVs) also remained ecologically
281 uncategorized. (**Fig. 3b**).

282 The phytoplankton community consisted of diatoms, green algae, haptophytes, and autotrophic
283 dinoflagellates, most of which were associated with ArW (**Fig. 4, Table S3**). In terms of read
284 abundance, *Thalassiosira* spp. and *Chaetoceros* sp. dominated among diatoms, while *Micromonas*
285 *polaris* was the dominant species within the green algae. The haptophytes group was primarily
286 represented by *Phaeocystis* sp., whereas the *Gymnodinium* spp. and sea-ice-associated species
287 *Polarella glacialis* were dominant within the autotrophic dinoflagellate group (**Fig. S4**). The
288 mixoplankton community was primarily composed of mixotrophic dinoflagellates and
289 silicoflagellates. In terms of read abundance, mixotrophic dinoflagellates were mainly present
290 from the Younger Dryas to the beginning of the Early Holocene, whereas mixotrophic
291 silicoflagellates, represented by *Pseudopedinella* sp., was present throughout the entire core (**Fig.**
292 **S4**).

293 The planktonic heterotrophic protists group included radiolarians, pelagic ciliates,
294 dinoflagellates, and silicoflagellates. These groups were identified as being present at specific time
295 periods, e.g. ~12.4 to ~10.2 kyr, and ~2.3 to 1.3 kyr BP (**Fig. S5, Table S3**). The mesozooplankton
296 group comprises small metazoans and was dominated by arthropods (Copepoda and Malacostraca)
297 and larvaceans (Appendicularia). The copepod *Calanus* spp. represented the majority of the
298 mesozooplankton around the study area (**Fig. S5**).

299 The zoobenthos was recorded as the most diverse group, primarily representing macrobenthic
300 species (**Fig. 4**). This group included annelids, ascidiacean, molluscs, cnidarians, and echinoderms

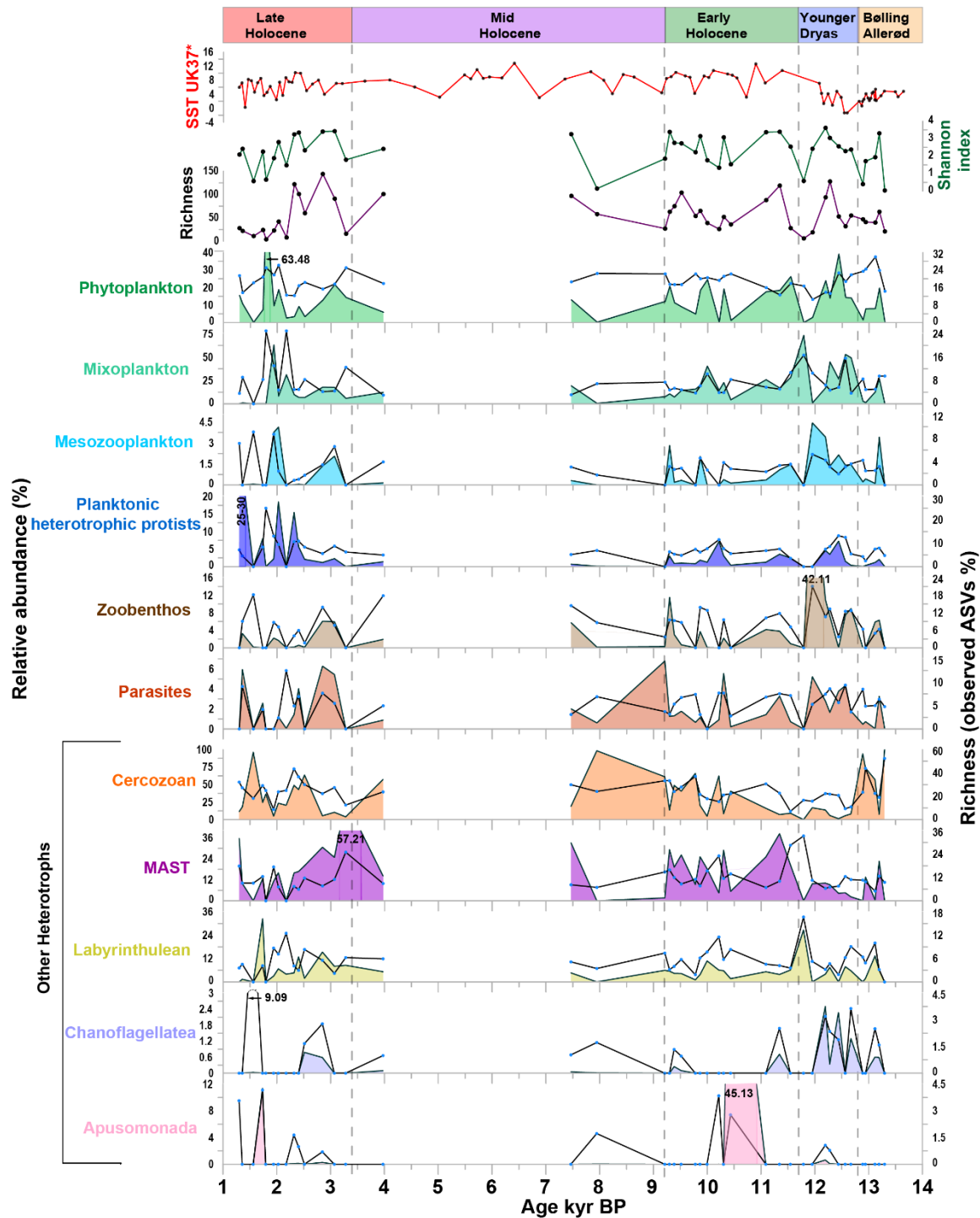
301 (Fig. S6, Table S3). Zoobenthos taxa were most abundant around ~9.3 kyr BP, as well as between
302 ~12.3 kyr and 12.0 kyr BP (Fig. 4).

303 The parasites were represented by six classes: Dinophyceae (Syndiniales), Gregarinomorphea,
304 Paragregarea, Peronospora, Hyphochytra, and Enoplea (Fig. 4, Table S3). Among them,
305 Syndiniales have the highest abundance and diversity, with 18 ASVs (mainly uncultured) detected
306 throughout the studied time interval (Fig. S7). The nekton group included two ASVs assigned to
307 Arctic cod (order Gnathostomata), which were detected only during the Younger Dryas and Early
308 Holocene.

309 Among other heterotrophs, Cercozoa were dominant, accounting for a significant proportion of
310 reads throughout the study period (Fig. 4, Table S3). Five classes of Cercozoa were identified:
311 Ascetosporea, Phytomyxea, Granofilosea, Thecofilosea, and Imbricatea. Thecofilosea exhibited
312 the highest richness with 51 ASVs (Fig. S8, Table S3). Ecologically, cercozoans can be classified
313 as parasitic, predatory, and bacterivorous. *Cryothecomonas* spp. were identified as predatory,
314 while those in the classes Ascetosporea and Phytomyxea were classified as parasites. Other
315 cercozoan ASVs were identified only to the family level, limiting precise ecological
316 interpretations.

317 The other heterotrophs also include the MAST (Marine Stramenopiles), Labyrinthulea,
318 Choanoflagellata and Apusomonada. The MAST group included 16 ASVs, representing four main
319 sub-clades: MAST-1, MAST-3, MAST-9, and MAST-12. MAST 9 and MAST 12 dominated
320 throughout the studied time period and exhibited high richness (Fig. S7, Table S3).

321 The Labyrinthulea included saprotrophic Thraustochytriaceae, and Aplanochytriidae, revealing
322 a dominant presence and high richness around ~11.8 kyr to ~2.2 kyr, and ~1.7 kyr BP (Fig. 4).
323 Most choanoflagellate ASVs belonged to environmental clades, except for *Calliacantha* sp., which
324 was dominated around ~12.7 kyr to ~12.2 kyr BP (Fig. 4). Apusomonada, represented by the class
325 Apusomonadea, appeared during certain time intervals, especially the Early Holocene (~10.4 kyr
326 BP), and Late Holocene (~1.7 kyr BP) (Fig. 4, Table S3). (see **Supplementary document** for
327 more details).



328

329 **Figure 4:** Relative abundance and richness (expressed as observed ASVs percentage) of major
 330 ecological groups, along with Shannon index, richness, and sea surface temperature [SST UK'37]
 331 from Łacka et al. [2019]. Lines represented ASVs abundance (%), and area represented the read
 332 abundance (%).

333

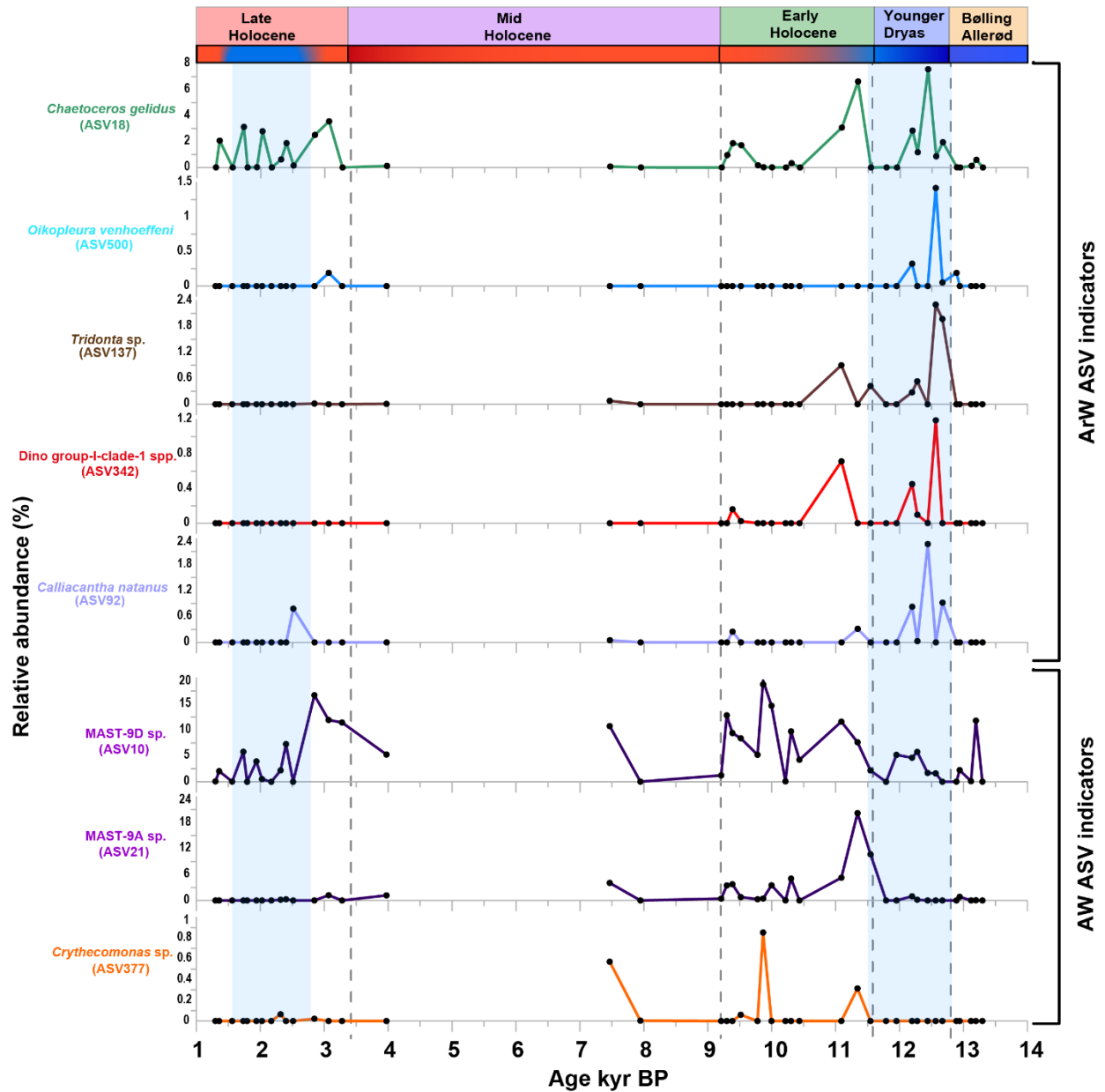
334 **4.5 Indicator taxa for Arctic and Atlantic water conditions**

335 A total of 44 ASVs were identified as potential indicator taxa using three analytical approaches
336 (sPLS, Spearman correlation, and DESeq) (**Fig. S9, S10, Table S5**). Of these, 16 ASVs were
337 identified as potential AW indicators, and belonged to the following groups: phytoplankton (1),
338 planktonic heterotrophic protists (1), cercozoans (6), MAST (3), zoobenthos (1), labyrinthulean
339 (1), and unassigned ASVs (1). The AW plankton indicators included a green algae *Pyramimonas*
340 sp. (ASV55), heterotrophs-Silicoflagellate *Pteridomonas* sp. (ASV105), and a pelagic ciliate
341 *Cyclotrichium* sp. (ASV265), while the AW benthic indicators comprised a polychaete *Tharyx* sp.
342 (ASV278) (**Fig. S11, Table S5**).

343 In contrast, 28 ASVs were associated with ArW (**Table S5**), primarily parasites (6), zoobenthos
344 (3), phytoplankton (4), choanoflagellates (1), planktonic heterotrophic protists (3),
345 mesozooplankton (1), mixoplankton (1), benthic ciliate (1), nekton (1), cercozoans (1), and
346 unassigned ASVs (6) (**Fig. S12, Table S5**). Potential ArW ASV-based indicators were identified
347 among both planktonic and benthic taxa. Planktonic ASVs comprised autotrophic dinoflagellates
348 (*Prorocentrum* sp., ASV64 and ASV153; *Gymnodinium* sp., ASV29), diatoms (*Chaetoceros*
349 *gelidus*, ASV18), mixotrophic dinoflagellate (*Heterocapsa rotundata*, ASV204), pelagic ciliate
350 (*Strombidium* sp., ASV123), radiolarian (*Heteracon* sp., ASV54; *Acanthoplegma* sp., ASV677),
351 and mesozooplankton (*Oikopleura* sp., ASV500). Parasites included three Syndiniales
352 dinoflagellates (ASV213, ASV341, and ASV391), an apicomplexan (*Paralecudina* sp., ASV958),
353 and a parasitic nematode (Mermithidae sp., ASV101). Benthic indicators included benthic ciliate
354 (*Holosticha* sp., ASV87), echinoderm (*Ctenodiscus* sp., ASV104), and bivalve (*Tridonta* sp.,
355 ASV137). Additionally, *Calliacanthea natans* (ASV92) was identified as an ArW indicator in our
356 study (**Table S5**).

357 Eight ASVs were identified as the most robust ASV-based indicators of AW and ArW
358 conditions, based on their consistent occurrence through time (detected in more than four samples)
359 and strong statistical support (correlation coefficient > 0.4; $p < 0.05$) (**Fig. 5**).

360

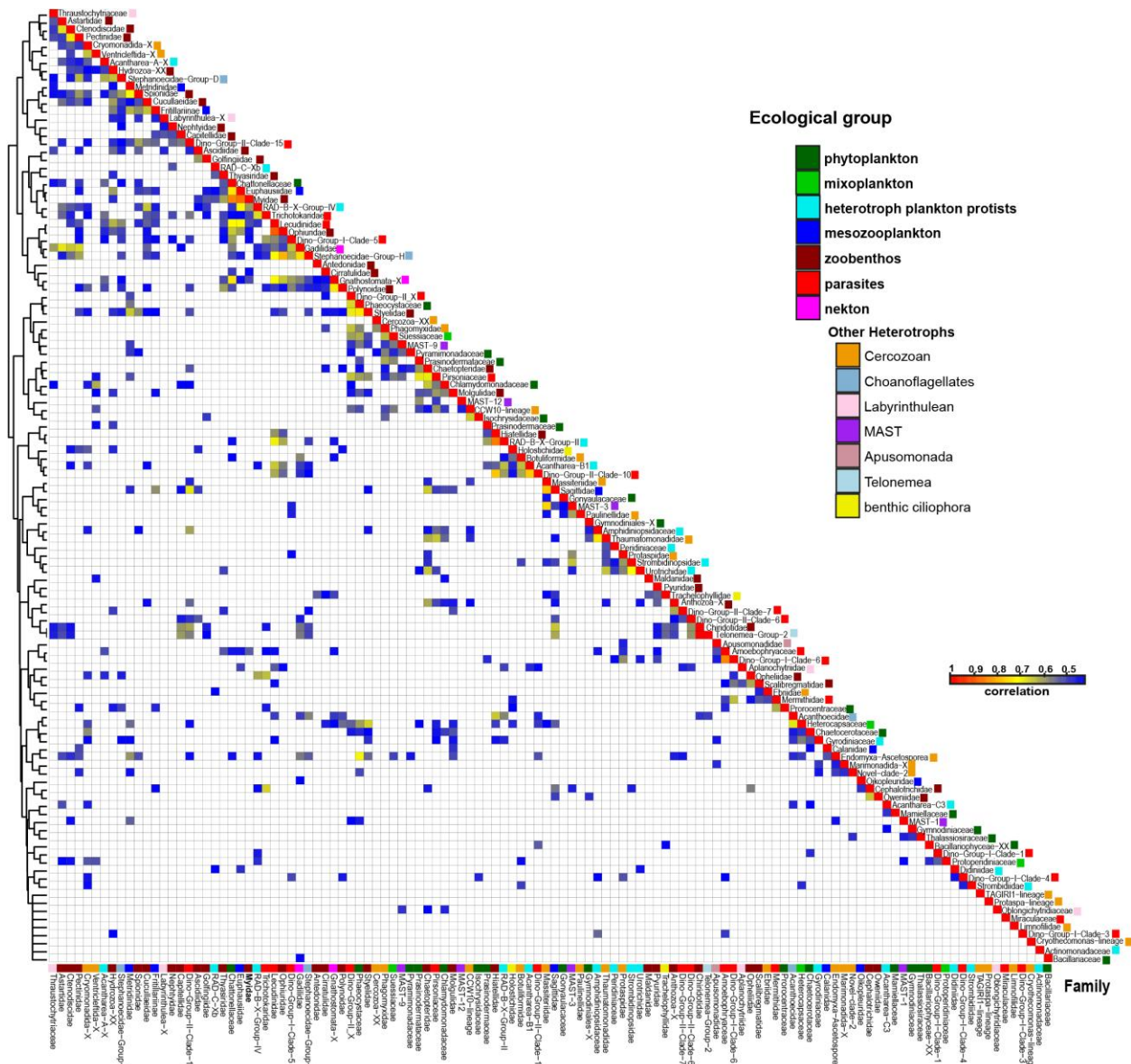


361
 362 **Figure 5:** Potential ASV-based indicators of AW and ArW conditions from the study (correlation
 363 >0.4 , $P < 0.05$, positive results from at least two method (displayed data as relative abundance %, and included the ASVs recorded in more than four samples).

365 4.6 Ecological interactions among eukaryote families

366 Spearman correlation analysis ($r > 0.5$, adjusted $p < 0.001$) was used to explore potential
 367 ecological interactions among eukaryotic families inhabiting similar environmental niches (**Fig. 6**,
 368 **Table S6**). Parasitic cercozoans (Ascetosporea and Phagomyxidae) strongly correlated with algae
 369 families (Phaeocystaceae, Thalassiosiraceae, Pyramimonadaceae, and Prasinodermataceae), and

370 dinoflagellates (Suessiaceae, and Gymnodiniaceae). Other cercozoans (CCW10-lineage, Novel-
371 Clade-2, Cryothecomonas-lineage, and Ventricleftida) revealed significant correlations with algal
372 and dinoflagellate groups (**Fig. 6, Table S6**). Among MAST groups, MAST-12 showed positive
373 associations with algae families (Prasinodermataceae, Thalassiosiraceae, and Chaetocerotaceae)
374 and parasites (Pirsoniaceae), while MAST-9 correlated with multiple phytoplankton families (**Fig.**
375 **6, Table S6**). Parasitic dinoflagellates (dino-group-II) showed strong correlation with haptophyte
376 algae (Phaeocystaceae), diatom (Thalassiosiraceae), and dinoflagellates (Suessiaceae, and
377 Gymnodiniaceae). Parasitic alveolates of the family Lecudinidae showed a strong positive
378 correlation with the mesozooplankton (Malacostraca), radiolarians and ophiuroids (**Fig. 6, Table**
379 **S6**). Another parasitic superfamily of Stramenopiles, the Pirsoniaceae displayed strong
380 associations with various taxa, including MAST-12, cercozoans (Thaumatomonadidae), green
381 algae (Prasinodermataceae, and Chlamydomonadales), haptophytes (Phaeocystaceae), diatoms
382 (Thalassiosiraceae), silicoflagellates (Actinomonadaceae), dinoflagellates
383 (Amphidiniopsidaceae), and polychaetae (Chaetopteridae) (**Fig.6, Table S6**).
384



385
 386 **Figure 6:** Heatmap of co-occurrence based on Spearman rank coefficient analysis between
 387 eukaryote families represent in the study (illustrated only the positive correlation ≥ 0.4 , and p value
 388 adjusted (BH) < 0.05).

389 **5. Discussion**

390 This study expands our knowledge of eukaryotic communities' patterns in the Storfjordrenna over
 391 the past 13,300 years by providing high-resolution sedaDNA records of both fossilized and non-
 392 fossilized groups. We demonstrate how these communities responded to major climatic shifts since
 393 the Bølling-Allerød and highlight key ecological interactions among major taxonomic groups.

394 These findings enhance our understanding of how environmental changes have shaped eukaryotic
395 biodiversity in southern Svalbard.

396 **5.1.Impacts of oceanographic changes on the eukaryotic community in Storfjordrenna**

397 **5.1.1 Bølling-Allerød (13.30 kyr BP to 12.80 kyr BP)**

398 The eukaryotic community in our record during the Bølling–Allerød reflected oceanographic
399 conditions resembling those observed today in glacier-proximal areas of Arctic fjords,
400 characterized by high turbidity due to meltwater discharge and the presence of colder, fresher
401 waters (Łącka et al., 2019; Zajączkowski, 2008). Previous studies support this interpretation: the
402 grounding line of the Svalbard Barents Ice Sheet (SBIS) retreated from Storfjordrenna before
403 13.95 kyr BP (Łącka et al., 2015), coinciding with SST reaching modern-like values (Łącka et al.,
404 2019). However, despite elevated SST, primary productivity remained low likely due to the
405 suppressive effect of turbid meltwater input from the retreating ice sheet (Łącka et al., 2015).
406 Furthermore, biomarker data indicated a dominance of fresher ArW over AW, which has been
407 linked to reduced primary productivity (Łącka et al., 2019). These conditions favored the
408 development of a eukaryotic community dominated by heterotrophs, capable of thriving in such
409 extreme environments. The most abundant taxa, in terms of both sequence reads and ASV richness,
410 were bacterivorous cercozoans (**Fig. 4**). The dominant cercozoan was *Limnofila* sp., a genus
411 primarily found in fresh and brackish waters (Mylnikov et al., 2015; Nikolaev et al., 2003), the
412 presence of *Limnofila* sp. may reflect either local ecological conditions or allochthonous input via
413 riverine transport or ice-rafted debris (Andruszkiewicz et al., 2019; Jo et al., 2025; Nguyen et al.,
414 2026). Other important bacterivorous heterotrophs were MAST, particularly MAST-9D and
415 MAST-12A, which are known to be adapted to extreme environmental conditions (Labarre et al.,
416 2021; Lin et al., 2022; Obiol et al., 2024).

417 Despite lower read abundance, phytoplankton, mixoplankton, and planktonic heterotrophic
418 protists showed high ASV richness during this period (**Fig. 4**). The phytoplankton community was
419 dominated by autotrophic, sea-ice associated taxa, such as dinoflagellates *Polarella glacialis*
420 (Harðardóttir et al., 2024) and *Gymnodinium* spp. (Kubiszyn and Wiktor, 2016), and diatom
421 *Thalassiosira* spp. (Luddington et al., 2016). The mixoplankton was represented by the
422 silicoflagellate, *Pseudopedinella elastica* (**Fig. S4**), which has been described as bacterivorous
423 under conditions of limited light and nutrients (Gerea et al., 2016). The mesozooplankton

424 community was primarily composed of the herbivorous *Calanus* spp. and the omnivorous *Metridia*
425 *longa*. These species have been previously observed in the Svalbard region, with *Calanus* spp.
426 dominating in terms of biomass (Daase et al., 2008). Despite unfavorable conditions caused by
427 meltwater influx and low nutrient availability, both primary and secondary productivity persisted,
428 likely concentrated in ice-proximal and frontal zones where the stratification enhanced nutrient
429 retention and water column stability (Łącka et al., 2019; Łącka et al., 2015). This suggests that
430 environments near retreating ice sheets can act as biological hotspots, supporting productivity
431 through ice-associated blooms and complex interactions within the microbial food web.

432 **5.1.2 Younger Dryas (12.80 kyr BP to 11.70 kyr BP)**

433 The eukaryotic community during the Younger Dryas reflected the dramatic environmental
434 changes that occurred at that time. The most notable change was the rapid decrease in biodiversity
435 during the Bølling-Allerød and Younger Dryas transition, when alpha diversity indices reached
436 near-zero values (**Fig. 4**). The reorganization of oceanographic conditions most likely caused a
437 temporary slowdown of Atlantic meridional overturning circulation (AMOC) and a reduction in
438 AW inflow (Łącka et al., 2020). This led to strong stratification, formation of perennial ice cover,
439 and anoxic conditions at the bottom (Łącka et al., 2020). The presence of perennial ice cover led
440 to a significant reduction in primary productivity in Storfjordrenna (Łącka et al., 2019). However,
441 the sedaDNA record also revealed the presence of phyto- and mixoplankton during this period,
442 especially presence of phytoplankton *Thalassiosira* spp. and *Gymnodinium* sp., and silicoflagellate
443 *P. elastica*. This may suggest that, although limited, primary productivity still occurred under the
444 ice. The detection of herbivorous mesozooplankton *Calanus* spp., and predatory *Cryothecomonas*
445 spp., also coincided with the presence of phytoplankton. Notably, the early Younger Dryas also
446 revealed a short-term increase in the relative abundance and diversity of zoobenthos, primarily
447 polychaetae (*Barantolla* sp.) and molluscs (*Tridonta* sp. and *Talochlamys* sp.) (**Fig. S6**).

448 During the latter part of the Younger Dryas (after ~12.4 kyr BP), increasing advection of AW
449 and SST warming led to the replacement of perennial sea ice by seasonal ice cover (Łącka et al.,
450 2019; Łącka et al., 2020). This shift was followed by the development of a more diverse benthic
451 foraminifera community (Łącka et al., 2015). Similarly, the sedaDNA record displayed the
452 increase in the richness and abundance of zoobenthic taxa, mainly annelids, molluscs, and
453 echinoderms (**Fig. S6**). However, the alkenone record suggested that the warming was may

454 associated with low primary productivity, probably due to the continuous input of turbid meltwater
455 from the decaying SBIS (Łącka et al., 2015).

456 In contrast, the sedaDNA record indicated a sudden phytoplankton bloom in the late Younger
457 Dryas, dominated by *M. polaris*, *Thalassiosira* spp., *Chaetoceros gelidus*, and *Gymnodinium* spp.
458 *Micromonas polaris* is typically associated with Arctic sea-ice environments (Bachy et al., 2022),
459 and was recorded during the periods of low SST. *Chaetoceros gelidus* is known for its high
460 tolerance under variable light and ocean acidification conditions (Biswas, 2022; Ribeiro et al.,
461 2024) and may play a key role in plankton blooms and primary productivity, particularly during
462 the Younger Dryas (**Fig. S4**). Phytoplankton blooms stimulated the development of secondary
463 producers, mainly pelagic ciliates, and radiolarians, as well as mesozooplankton copepods
464 (*Calanus* spp.) (**Fig. S5**). Altogether, these findings indicate that the latter part of the Younger
465 Dryas (after ~12.4 kyr BP) was characterized by periods of accelerated AW inflow and higher SST
466 (Risebrobakken et al., 2010; Wollenburg et al., 2004), which promoted phytoplankton and
467 zooplankton growth, and enhanced development of the benthic community.

468 **5.1.3 Early Holocene (11.70 kyr BP to 9.20 kyr BP)**

469 The transition from the Younger Dryas to the Early Holocene was characterized by a significant
470 decrease in biodiversity and the dominance of mixoplankton, primarily silicoflagellate *P. elastica*,
471 and dinoflagellates such as *Biecheleria* sp. and *Gotoius* sp. According to Łącka et al., (2020), the
472 onset of the Early Holocene was associated with a short-term decrease in SST and a decrease in
473 foraminiferal fauna abundance. The low biodiversity and dominance of mixotrophic plankton
474 observed in the sedaDNA record might be a consequence of this short-term deterioration in
475 environmental conditions.

476 However, the further development of the Early Holocene was driven by an increasing influence
477 of AW in the area, which was followed by an increase in SST and productivity (Devendra et al.,
478 2023; Telesiński et al., 2018). Moreover, Arctic Front was located close to the Spitsbergen coast,
479 leading to the formation of a highly productive frontal zone (Łącka et al., 2019). The amelioration
480 of environmental conditions during the Early Holocene (Łącka et al., 2015) was reflected in a
481 sudden peak of alpha diversity of overall eukaryotic community, accompanied by a notable
482 increase in the richness and abundance of key ecological groups, including phytoplankton,
483 zoobenthos, parasites, and other heterotrophs such as cercozoans and MAST (**Fig. 4**). However,
484 taxa associated with sea-ice were an important component of the assemblage, suggesting that sea-

485 ice formation still occurred in Storfjordrenna. Despite AW dominance, the presence of a brackish
486 water cercozoan *Limnofila* sp., green algae *M. polaris* and *Pyramimonas* sp., as well as sea-ice-
487 indicator *P. glacialis* may suggest episodic presence of sea-ice, and transition of Arctic Front (**Fig.**
488 **S4, S8**). The overall high eukaryotic biodiversity in the Early Holocene, particularly the diversity
489 of phytoplankton, mixoplankton, mesozooplankton, and the gradual increase in MAST-9 species
490 related to warm water further support the establishment of warm-water conditions with high
491 nutrient availability (Łączka et al., 2019) (**Fig S4, S5, S7, and Table S5**).

492 **5.1.4 Mid Holocene (9.20 kyr BP to 3.40 kyr BP)**

493 Samples from the Mid Holocene, spanning the period between 4.0 and 7.5 kyr BP, show low
494 eukaryote DNA recovery, likely due to extensive degradation, and are dominated by fungi and
495 amoebozoan DNA, particularly *Acanthamoeba*, which constitutes a large proportion of the
496 recovered sequences. The dominance of amoebozoan DNA may reflect elevated microbial activity,
497 potentially accelerating post-depositional DNA degradation (Anderson, 2017; Boere et al., 2011;
498 Butler and Rogerson, 1995). As a result, lack of eukaryotic sedaDNA data from the period between
499 ~7.5 and 4.0 kyr BP (see Results), restricting interpretation to the early Mid Holocene and the
500 transition toward the Late Holocene. Therefore, this interpretation should be treated with caution
501 due to the limited number of samples analyzed in this interval. The beginning of the Mid Holocene
502 (9.2 kyr BP) in Storfjordrenna was marked by a significant drop in biodiversity, followed by an
503 increase after 8.0 kyr BP. The species composition was predominantly composed of cercozoans,
504 mainly *Limnofila* sp. and *Cryothecomonas* spp. (**Fig. S8**). Another important component of the
505 eukaryotic assemblage was MAST species, including MAST-9D and MAST-12B, which had
506 previously been recorded in the north Atlantic region (Lopez-Garcia et al., 2007; Newbold et al.,
507 2012) (**Fig. S7**). The community composition resembled the one from Bølling Allerød, dominated
508 by heterotrophic taxa adapted to unfavorable environmental conditions. This aligns with evidence
509 of a minor cooling event between 9.0 kyr and 8.0 kyr BP, as proposed in previous studies (Łączka
510 et al., 2015).

511 In contrast, despite their relatively low abundance, the communities of phytoplankton,
512 mesozooplankton, and planktonic heterotrophic protists displayed relatively high diversity in the
513 early Mid-Holocene. This period in Storfjordrenna was characterized by limited ice rafting,
514 variable SST, and interplay between the AW and ArW water masses rather than a continuous

515 impact of AW (Łacka et al., 2019; Łacka et al., 2015). Furthermore, the low alkenone flux indicated
516 low primary productivity throughout the mid-Holocene (Łacka et al., 2019), which is consistent
517 with the reduced representation of both phyto- and zooplankton taxa in the sedaDNA record and
518 supports an interpretation of sustained low productivity–related community signals during this
519 interval. Low productivity was also observed at that time in the Norwegian and Svalbard shelves,
520 potentially due to the limited nutrient availability. According to Łacka et al., (2019), the reduction
521 in primary productivity resulted from enhanced vertical stratification, which reduced vertical
522 mixing in the water column, and thus, limited the nutrient resuspension to the surface. An
523 alternative explanation is the early spring bloom, that occurs in the ice-free waters, and the
524 subsequent development of mesozooplankton that graze on phytoplankton, thereby reducing the
525 flux of organic matter to the bottom. However, the presence of low abundance sequences assigned
526 to both phytoplankton and planktonic heterotrophic protists, as well as the increase in
527 bacterivorous taxa, likely supports the first scenario. Overall, the lack of sea ice, and the variability
528 in water masses and SST observed at the beginning of the Mid Holocene, created an unstable
529 environment, which favored tolerant heterotrophic eukaryotes such as cercozoans or MAST.

530 **5.1.5 Late Holocene (3.40 kyr BP to 1.30 kyr BP)**

531 The onset of the Late Holocene was marked by an increase in eukaryotic biodiversity, followed
532 by a sharp decrease around 2.0 kyr BP. During this period, eukaryotic communities were
533 predominantly composed of cercozoan and MAST (**Fig. 4**). Cercozoan abundance and richness
534 exhibited an increasing, yet variable trend throughout the Late Holocene, whereas MAST
535 decreased progressively over time.

536 Both phytoplankton and planktonic heterotrophic protists exhibited high richness, but variable
537 abundance throughout the Late Holocene (**Fig. 4**). Furthermore, the presence of parasitic species,
538 including the Syndiniales dinoflagellate (dino-group-I and dino-group-II) as well as the diatom-
539 associated parasitic *Pirsonia* sp. (Schweikert and Schnepf, 1997), co-occurred with the
540 phytoplankton suggesting that parasitic interactions may have influenced phytoplankton dynamics
541 during the Late Holocene. (**Fig. S7, Table S6**). The Late Holocene coincided with the so-called
542 Neoglacial cooling, which spanned the last 4.0 kyr BP. This period was characterized by a decline
543 in SST (Risebrobakken et al., 2010), limited AW inflow and strengthening of ArW flow, which led
544 to the formation of extensive ice cover (Berben et al., 2014; Devendra et al., 2023; Martrat et al.,
545 2003). Records from Storfjordrenna also showed a cooling in the area, associated with enhanced

546 ice rafting (Łącka et al., 2019; Łącka et al., 2015). Thus, the increased abundance of phytoplankton
547 in general, and ice-associated species *P. glacialis* in particular, is probably an effect of the cooling
548 of surface waters and the formation of sea-ice, which launched convective water mixing and
549 nutrient resuspension to the surface. In consequence, primary productivity increased, stimulating
550 the development of the planktonic heterotrophic protists community (**Fig. S5**).

551 **5.2. sedaDNA environmental indicators**

552 This study identified 46 potential eukaryotic indicator taxa associated with AW and ArW
553 conditions. Several of these taxa exhibited consistent temporal patterns that aligned with
554 paleoenvironmental proxies, supporting their potential for long-term reconstructions. In contrast,
555 others appeared only sporadically, which reduces their reliability as potential indicators. AW-
556 associated taxa were primarily represented by cercozoans and MAST, while ArW-associated taxa
557 included diatoms, dinoflagellates, choanoflagellates, Arctic zoobenthos, and zooplankton.

558 Bacterivorous cercozoans, including the Ventricleftida (ASV46), the Protaspa-lineage (ASV83,
559 and ASV257), Ventricleftida spp. (ASV46) and the *Cryothecomonas* spp. (ASV377), were
560 identified as potential AW indicators (**Fig. S11, Table S5**). However, their identification is
561 currently based exclusively on molecular data, limiting ecological and biogeographical context
562 and weakening their use in environmental reconstructions (Labarre et al., 2021; Obiol et al., 2024).
563 Similarly, members of the bacterivorous MAST-9 group, notably MAST-9A and MAST-9D, were
564 exclusively detected in AW conditions (**Fig. 5, Table S5**), which is consistent with their known
565 tropical-to-temperate distribution. Within the phytoplankton communities, *Pyramimonas parkeae*
566 (a green alga that prefers higher temperature regions; (Bock et al., 2021)), and the planktonic
567 heterotrophic pelagic ciliate *Cyclotrichium* sp. (commonly found in warmer waters; (Dirmenci et
568 al., 2010; Xu et al., 2005)), were also identified as potential AW indicators. However, they only
569 occurred in a brief temporal window near the end of the Early Holocene, so their reliability as
570 indicators needs to be verified by further studies (**Fig. S11**).

571 The relatively high number of cold-water species recorded was probably due to favorable
572 overall conditions in the study area. The autotrophic *Prorocentrum* spp. are known to be toxin-
573 producing, bloom-forming species with broad global distributions, including polar regions (Cen et
574 al., 2020; Goncharenko et al., 2021; Stoecker and Lavrentyev, 2018; Tillmann et al., 2022). In the
575 present study, both taxa were primarily detected at the onset of the Younger Dryas (**Table S6**).
576 Their limited distribution suggests that they may be unreliable as long-term environmental

577 indicators. Similarly, *Heterocapsa rotundata* a mixotrophic dinoflagellate commonly associated
578 with harmful algal blooms in Arctic and North Atlantic waters (Rintala et al., 2010; Wu et al.,
579 2022), was identified as a potential ArW indicator (**Fig. S12**). The genus *Holosticha* is a
580 widespread benthic ciliate, associated with sea ice (Berger, 2003; Petz et al., 1995; Wilbert and
581 Song, 2008), and known to feed on diatoms and flagellates (Lei et al., 2005), which was also
582 identified as a potential ArW indicator (**Fig. S12**). However, their presence was confined to the
583 Bølling-Allerød and Younger Dryas or the Younger Dryas and Early Holocene intervals,
584 respectively, limiting their reliability as a long-term proxy for ArW conditions (**Fig. S12**).

585 In contrast, the ArW-associated diatom species *Chaetoceros gelidus* was consistently abundant,
586 (**Fig. 5**), contributing to bloom formation and demonstrating adaptability to low light conditions
587 (Biswas, 2022; Hoppe et al., 2018). Among the zooplankton, two taxa were identified as potential
588 indicators: the planktonic heterotrophic radiolarian species *Heteracon* sp. and the
589 mesozooplankton filter feeder appendicularian *Oikopleura vanhoeffeni* (Deibel, 1986, 1988)(**Fig.**
590 **5**). Likewise, the cold-water bivalve species *Tridonta* sp. which is commonly found in the North
591 Atlantic and Arctic region (Marincovich Jr et al., 2002; Petersen, 2001), demonstrated strong
592 potential as an indicator species. Within parasitic dinoflagellates, three potential indicators
593 belonging to dino-group-I, mostly associated with sea-ice conditions (Clarke et al., 2019), were
594 identified (**Fig. S12**). Choanoflagellate recorded in the study can be identified as a sea-ice
595 associated group due to the presence of potential ArW indicator taxa (Buck and Garrison, 1988;
596 Thomsen and Østergaard, 2017) (**Fig. 5**). These taxa were all consistently present throughout the
597 study period, suggesting a stable association with cold marine conditions.

598 *C. gelidus*, *O. vanhoeffeni*, *C. natans*, Dino-group-I-clade-I spp., and *Tridonta* sp. exhibited the
599 strongest ArW indicator potential, reflected by their consistent detection across samples and their
600 concordant associations with multiple independent paleoenvironmental proxies. In contrast,
601 MAST-9D sp., MAST-9A sp., and *Cryothecomonas* spp. showed the strongest indicators of AW
602 influence. (**Fig. 5**). However, their Spearman correlation coefficients between environmental
603 variables ranged from 0.3 to 0.6 ($p < 0.05$), indicating a weak to moderate association. This may
604 be due to a combination of interspecific competition and the influence of multiple external
605 environmental variables in the study area. These interacting factors contribute to the complexity
606 of the ecosystem and limit the effectiveness of using single-proxy approaches when interpreting
607 the responses of indicator species in paleoenvironmental reconstructions. Further studies of

608 eukaryotic communities in other Arctic regions are therefore needed to validate these taxa as robust
609 indicator species.

610 **5.3. Interactions within eukaryotic community structure in Storfjordrenna**

611 The biodiversity of eukaryotic communities in Storfjordrenna was previously influenced by the
612 interplay between ArW and AW masses, as well as sea-ice coverage over the past 13.30 kyr BP.
613 Throughout the study period, eukaryotic alpha diversity remained relatively stable, with a notable
614 exception during the transitions between major climatic intervals suggesting that these changes
615 were driven primarily by species replacement, rather than by loss of richness or evenness (**Fig. 4,**
616 **Fig. S2**). This may imply that key trophic interactions and ecosystem functions persisted, reflecting
617 functional resilience of Storfjordrenna eukaryotic communities during periods of environmental
618 change. Notably, biodiversity peaks coincided with the presence of sea-ice margins and frontal
619 zones, environments known to promote phytoplankton growth and primary productivity (**Fig. 4**).

620 Analysis of phytoplankton diversity revealed a consistent presence of green algae throughout
621 the study period, except during the Bølling Allerød interstadial, when diatoms dominated.
622 Taxonomic abundance showed dynamic fluctuations, with gradual declines observed during the
623 transitions between major climatic intervals. This suggests that environmental instability may have
624 influenced the structure of the phytoplankton community.

625 Key contributors to primary productivity in the Storfjordrenna were diatoms (*Thalassiosira*
626 spp., and *Chaetoceros* spp.), green algae (*M. polaris*), and autotrophic dinoflagellates (*P. glacialis*,
627 and *Gymnodinium* spp.). Additionally, Spearman rank correlation analysis showed that the family
628 Actinomonadaceae, mainly represented by *Pseudopedinella* sp., was positively associated with
629 diatoms. Spearman rank correlation analysis also revealed a positive association between parasitic
630 cercozoans and phytoplankton communities (**Fig. 6, Table S6**), indicating that the presence of
631 parasitic cercozoans may play a significant role in shaping ecological interactions within
632 phytoplankton assemblages (Bass et al., 2009; Cavalier-Smith and Chao, 2003; Hartikainen et al.,
633 2014). Conversely, the parasitic apicomplexan family Lecudinidae was associated with zoobenthos
634 (e.g., Heteroconchia and Ophiurida) and mesozooplankton (e.g., Malacostraca), may highlight
635 their parasitic relationships with marine invertebrates (Rueckert et al., 2015) (**Fig. 6, Table S6**).
636 Parasitic dinoflagellates (dino-group-II) were positively associated with haptophytes and diatoms.
637 The parasitic nanoflagellate Pirsoniaceae: *Pirsonia* sp., demonstrated a positive correlation with

638 autotrophic microbes, including, dinoflagellates, diatoms, and silicoflagellates (Kühn et al., 2004;
639 Schweikert and Schnepf, 1997). This raises questions about the nature of their ecological
640 interactions, and whether they are strictly parasitic or co-occur under similar environmental
641 conditions. These findings emphasize the need for further investigation to understand the
642 mechanisms driving these interactions and their broader implications for microbial community
643 dynamics.

644 Cercozoans have emerged as the most dominant group within the eukaryotic community, in
645 terms of both abundance and species richness. Cercozoan community included taxa previously
646 recorded in various habitats including fresh and marine environments (Chantangsi and Leander,
647 2010; Irwin et al., 2019). Their occurrence across a wide range of environmental conditions
648 highlights their ecological flexibility and broad tolerance. Although cercozoans as a group exhibit
649 high richness, only a few lineages, such as the Imbricata-novel clade 2, *Protaspa* spp.,
650 *Cryothecomonas* spp., and Ascetosporea, persisted consistently throughout the study period, while
651 most of the others were restricted to specific time intervals (**Fig. S8**). This suggests that, although
652 cercozoans as a whole group may not be sensitive to environmental shifts, individual lineages are
653 likely to be more responsive.

654 MAST species constituted a major microbial group within the eukaryotic community, with
655 MAST-9 dominant overall and MAST-12 particularly prevalent during the late Holocene. These
656 two MAST subgroups are commonly associated with temperate regions or extreme environments
657 such as cold seeps (Lin et al., 2022; Obiol et al., 2024). The statistical analysis identified potential
658 warm-water indicator species within these groups (**Fig. 5, Table S5**). Based on the co-occurrence
659 relation, the MAST-12, and MAST-9 subgroup revealed a positive correlation (> 0.6) with the
660 parasitic family of Pirsoniaceae and the phytoplankton families (**Fig. 6, Table S6**), providing
661 insight into their ecological activities within the eukaryotic community. Further analysis of the
662 ecological traits and distribution of micro eukaryotic taxa, mainly cercozoans and MAST, could
663 provide deeper insights into their ecological responses within the Storfjordrenna ecosystem.

664 **6. Conclusions**

665 Using sedaDNA metabarcoding, we reconstructed the paleoecology of eukaryotic
666 communities in Storfjordrenna over the last 13.30 kyr BP, elucidating their sensitivity and
667 adaptability to environmental variables. Most eukaryotic ASVs were assigned ecological

668 functional roles via higher taxonomic classification, considered reliable due to extensive ribosomal
669 reference databases. However, taxa with complex life cycles (e.g., dinoflagellates, ciliates)
670 required genus/species-level identification for more accurate functional assignment, necessitating
671 a cautious approach. While some classification errors are inevitable, their proportion in the dataset
672 is expected to be minimal. Overall, the eukaryotic biodiversity in Storfjordrenna remained
673 relatively stable, except during transitions between major climatic intervals, indicating that
674 community changes were primarily driven by species replacement rather than loss of richness or
675 evenness, which maintained ecosystem function. Peaks of biodiversity coincided with the presence
676 of sea-ice margins and frontal zones; environments known to foster favorable conditions for
677 phytoplankton development. Cercozoans and MAST emerged as dominant groups, demonstrating
678 their ecological flexibility and broad tolerance. This study revealed that primary productivity in
679 the Storfjordrenna region was mainly driven by phytoplankton, including diatoms (*Thalassiosira*
680 spp., *Chaetoceros* spp.), green algae (*Micromonas* spp.), and autotrophs dinoflagellates (*P.*
681 *glacialis*,) as well as mixoplankton species such as *Pseudopedinella elastica*. Our approach
682 revealed that, despite significant species turnover, functional diversity and ecosystem functions
683 remained largely stable, highlighting the resilience of Arctic planktonic communities. Several
684 potential ASV-indicators were identified through multi-method analyses, including taxa associated
685 with specific water masses. Our findings also underscore the complex interplay of environmental
686 drivers shaping community composition, revealing both positive and negative associations among
687 key microbial taxa. Our findings highlight the potential of sedaDNA for reconstructing past
688 eukaryotic communities and detecting environmental change. However, to fully unlock the
689 potential of sedaDNA approach in palaeoecological studies, it is essential to develop reference
690 databases for accurate and precise taxonomic identification of sequences, and to provide modern
691 reference data on the ecology and distribution of Arctic microbial eukaryotes. Therefore,
692 improving taxonomic resolution and validating indicator taxa remain essential for establishing
693 robust palaeoecological indicators in Storfjordrenna and the broader Svalbard region.

694

695 **Data availability.** Raw reads of 18S-V1V2 rDNA sequencing generated in this study were
696 deposited in the National Center for Biotechnology Information (NCBI) under Bio Project
697 PRJNA1299363, and the remaining data and additional details used for this study can be found in

698 the Supplement tables (**Table S1-S6**), Supplementary figures (**S1-S12**), and Supplementary
699 document.

700 **Supplement.** The supplement related to this article is available online at XXX.

701 **Author contributions.** **HN** and Joanna **P**, designed the study. Joanna **P** extract the DNA. **HN**
702 analyzed the DNA data, and performed bioinformatic, statistical analyses, and interpret the results.
703 Joanna **P**, Jan **P** and **N-LN** helped with the bioinformatic analysis, and interpret the results. **MŁ**
704 and **DD** help to clarify the age depth model, and the paleoenvironmental data. **HN** drafted the
705 paper, and prepared the figures, and tables. All authors contributed to data interpretation and
706 writing of the manuscript.

707 **Competing interests.** The contact author has declared that none of the authors has any competing
708 interests.

709 **Acknowledgements.** We thank the captain and crew of R/V Jan Mayen, as well as the cruise
710 participants, in particular Steinar Iversen, for their help at sea.

711 **Financial support.** The research was financially supported by the National Science Centre in
712 Poland through project 2022/47/B/ST10/03050.

713 **7. Reference**

714

715 Anderson, O. R.: Amoebozoan Lobose Amoebae (Tubulinea, Flabellinea, and Others), in: Handbook of the
716 Protists, edited by: Archibald, J. M., Simpson, A. G. B., and Slamovits, C. H., Springer International
717 Publishing, Cham, 1279-1309, https://doi.org/10.1007/978-3-319-28149-0_2, 2017.

718 Andruszkiewicz, E. A., Koseff, J. R., Fringer, O. B., Ouellette, N. T., Lowe, A. B., Edwards, C. A., and
719 Boehm, A. B.: Modeling Environmental DNA Transport in the Coastal Ocean Using Lagrangian Particle
720 Tracking, *Front. Mar. Sci.*, 6, <https://doi.org/10.3389/fmars.2019.00477>, 2019.

721 Armbrecht, L.: The Potential of Sedimentary Ancient DNA to Reconstruct Past Ocean Ecosystems,
722 *Oceanogr.*, 33, <https://doi.org/10.5670/oceanog.2020>, 2020.

723 Årthun, M., Eldevik, T., Smedsrud, L. H., Skagseth, Ø., and Ingvaldsen, R. B.: Quantifying the Influence
724 of Atlantic Heat on Barents Sea Ice Variability and Retreat, *J. Clim.*, 25, 4736-4743,
725 <https://doi.org/10.1175/JCLI-D-11-00466.1>, 2012.

726 Bachy, C., Sudek, L., Choi, C. J., Eckmann, C. A., Nöthig, E. M., Metfies, K., and Worden, A. Z.:
727 Phytoplankton Surveys in the Arctic Fram Strait Demonstrate the Tiny Eukaryotic Alga *Micromonas* and
728 Other Picoprasinophytes Contribute to Deep Sea Export, *Microbe.*, 10, 961,
729 <https://doi.org/10.3390/microorganisms10050961>, 2022.

730 Bass, D., Chao, E. E. Y., Nikolaev, S. I., Yabuki, A., Ishida, K., Berney, C., Pakzad, U., Wylezich, C., and
731 Cavalier-Smith, T.: Phylogeny of novel naked filose and reticulose Cercozoa: Granofilosea cl. n. and
732 Proteomyxidea revised, *Protist*, 160, 75-109, <https://doi.org/10.1016/j.protis.2008.07.002>, 2009.

733 Benner, I., Irwin, A. J., and Finkel, Z. V.: Capacity of the common Arctic picoeukaryote *Micromonas* to
734 adapt to a warming ocean, *Limnol. Oceanogr. Lett.*, 5, 221-227, <https://doi.org/10.1002/lol2.10133>, 2019.

735 Bensi, M., Nilsen, F., Ferre, B., Skogseth, R., Moskalik, M., Korhonen, M., Vogedes, D., Kovacevic, V., de
736 Mendoza, F. P., and Ingrosso, G.: The Atlantification process in Svalbard: a broad view from the SIOS
737 Marine Infrastructure network (ARiS)8293871148, 138-151, <https://doi.org/10.5281/zenodo.14425672>,
738 2024.

739 Berben, S. M. P., Husum, K., Cabedo-Sanz, P., and Belt, S. T.: Holocene sub-centennial evolution of
740 Atlantic water inflow and sea ice distribution in the western Barents Sea, *Clim. Past.*, 10, 181-198,
741 <https://doi.org/10.5194/cp-10-181-2014>, 2014.

742 Berger, H.: Redefinition of *Holosticha* Wrzesniowski, 1877 (Ciliophora, Hypotricha), *Eur. J. Protistol.*, 39,
743 373-379, <https://doi.org/10.1078/0932-4739-00006>, 2003.

744 Biswas, H.: A story of resilience: Arctic diatom *Chaetoceros gelidus* exhibited high physiological plasticity
745 to changing CO₂ and light levels, *Front. Plant. Sci.*, 13, 1028544,
746 <https://doi.org/10.3389/fpls.2022.1028544>, 2022.

747 Blindheim, J. and Østerhus, S.: The Nordic Seas, Main Oceanographic Features, in: *The Nordic Seas: An*
748 *Integrated Perspective*, 11-37, <https://doi.org/10.1029/158GM03>, 2005.

749 Bock, N. A., Charvet, S., Burns, J., Gyaltsen, Y., Rozenberg, A., Duhamel, S., and Kim, E.: Experimental
750 identification and in silico prediction of bacterivory in green algae, *ISME J.*, 15, 1987-2000,
751 <https://doi.org/10.1038/s41396-021-00899-w>, 2021.

752 Boere, A. C., Sinninghe Damsté, J. S., Rijpstra, W. I. C., Volkman, J. K., and Coolen, M. J. L.: Source-
753 specific variability in post-depositional DNA preservation with potential implications for DNA based
754 paleoecological records, *Org. Geochem.*, 42, 1216-1225,
755 <https://doi.org/10.1016/j.orggeochem.2011.08.005>, 2011.

756 Buck, K. R. and Garrison, D. L.: Distribution and abundance of choanoflagellates (*Acanthoecidae*) across
757 the ice-edge zone in the Weddell Sea, Antarctica, *Mar. Biol.*, 98, 263-269,
758 <https://doi.org/10.1007/Bf00391204>, 1988.

759 Butler, H. and Rogerson, A.: Temporal and Spatial Abundance of Naked Amoebae (Gymnamoebae) in
760 Marine Benthic Sediments of the Clyde Sea Area, Scotland, *J. Eukaryot. Microbiol.*, 42, 724-730,
761 <https://doi.org/10.1111/j.1550-7408.1995.tb01624.x>, 1995.

762 Callahan, B. J., McMurdie, P. J., Rosen, M. J., Han, A. W., Johnson, A. J., and Holmes, S. P.: DADA2: High
763 resolution sample inference from amplicon data, *Nat. Methods*, 13, 581-583,
764 <https://doi.org/10.1038/nmeth.3869>, 2015.

765 Cavalier-Smith, T. and Chao, E. E. Y.: Phylogeny and classification of phylum Cercozoa (Protozoa), *Protist*,
766 154, 341-358, <https://doi.org/10.1078/143446103322454112>, 2003.

767 Cen, J., Wang, J., Huang, L., Ding, G., Qi, Y., Cao, R., Cui, L., and Lü, S.: Who is the “murderer” of the
768 bloom in coastal waters of Fujian, China, in 2019?, *J. Oceanol. Limnol.*, 38, 722-732,
769 <https://doi.org/10.1007/s00343-019-9178-6>, 2020.

770 Chantangsi, C. and Leander, B. S.: An SSU rDNA barcoding approach to the diversity of marine interstitial
771 cercozoans, including descriptions of four novel genera and nine novel species, *Int. J. Syst. Evol.*
772 *Microbiol.*, 60, 1962-1977, <https://doi.org/10.1099/ijs.0.013888-0>, 2010.

773 Clarke, L. J., Bestley, S., Bissett, A., and Deagle, B. E.: A globally distributed Syndiniales parasite
774 dominates the Southern Ocean micro-eukaryote community near the sea-ice edge, *ISME J.*, 13, 734-737,
775 <https://doi.org/10.1038/s41396-018-0306-7>, 2019.

776 Daase, M., Eiane, K., Aksnes, D. L., and Vogedes, D.: Vertical distribution of *Calanus* spp. and *Metridia*
777 *longa* at four Arctic locations, *Mar. Biol. Res.*, 4, 193-207, <https://doi.org/10.1080/17451000801907948>,
778 2008.

779 Deb, J. C. and Bailey, S. A.: Arctic marine ecosystems face increasing climate stress, *Environ Rev.*, 31,
780 403-451, <https://doi.org/10.1139/er-2022-0101>, 2023.

781 Deibel, D.: Feeding mechanism and house of the appendicularian *Oikopleura vanhoeffeni*, *Mar. Biol.*, 93,
782 429-436, <https://doi.org/10.1007/Bf00401110>, 1986.

783 Deibel, D.: Filter feeding by *Oikopleura vanhoeffeni*: grazing impact on suspended particles in cold ocean
784 waters, *Mar. Biol.*, 99, 177-186, <https://doi.org/10.1007/Bf00391979>, 1988.

785 Devendra, D., Łącka, M., Szymańska, N., Szymczak-Żyła, M., Krajewska, M., Weiner, A. K. M., De
786 Schepper, S., Simon, M. H., and Zajączkowski, M.: The development of ocean currents and the response
787 of the cryosphere on the Southwest Svalbard shelf over the Holocene, *Glob. Planet. Change.*, 228, 104213,
788 <https://doi.org/10.1016/j.gloplacha.2023.104213>, 2023.

789 Dirmenci, T., Dündar, E., Deniz, G., Arabaci, T., Martin, E., and Jamzad, Z.: Morphological, karyological
790 and phylogenetic evaluation of *Cyclotrichium*: a piece in the tribe Mentheae puzzle, *Turk. J. Bot.*, 34, 159-
791 170, <https://doi.org/10.3906/bot-0912-3>, 2010.

792 Dufresne, Y., Lejzerowicz, F., Perret-Gentil, L. A., Pawlowski, J., and Cordier, T.: SLIM: a flexible web
793 application for the reproducible processing of environmental DNA metabarcoding data, *BMC Bioinform.*,
794 20, <https://doi.org/10.1186/s12859-019-2663-2>, 2019.

795 Esling, P., Lejzerowicz, F., and Pawlowski, J.: Accurate multiplexing and filtering for high-throughput
796 amplicon-sequencing, *Nucleic Acids Res.*, 43, 2513-2524, <https://doi.org/10.1093/nar/gkv107>, 2015.

797 Fonseca, V. G., Carvalho, G. R., Sung, W., Johnson, H. F., Power, D. M., Neill, S. P., Packer, M., Blaxter,
798 M. L., Lamshead, P. J. D., Thomas, W. K., and Creer, S.: Second-generation environmental sequencing
799 unmasks marine metazoan biodiversity, *Nat. Commun.*, 1, 98, <https://doi.org/10.1038/ncomms1095>, 2010.

800 Froslev, T. G., Kjoller, R., Bruun, H. H., Ejrnaes, R., Brunbjerg, A. K., Pietroni, C., and Hansen, A. J.:
801 Algorithm for post-clustering curation of DNA amplicon data yields reliable biodiversity estimates, *Nat.*
802 *Commun.*, 8, 1188, <https://doi.org/10.1038/s41467-017-01312-x>, 2017.

803 Gereá, M., Saad, J. F., Izaguirre, I., Queimaliños, C., Gasol, J. M., and Unrein, F.: Presence, abundance and
804 bacterivory of the mixotrophic algae *Pseudopedinella* (Dictyochophyceae) in freshwater environments,
805 *Aquat. Microbe. Ecol.*, 76, 219-232, <https://doi.org/10.3354/ame01780>, 2016.

806 Goncharenko, I., Krakhmalnyi, M., Velikova, V., Ascencio, E., and Krakhmalnyi, A.: Ecological niche
807 modeling of toxic dinoflagellate *Prorocentrum cordatum* in the Black Sea, *Ecohydrol. Hydrobiol.*, 21, 747-
808 759, <https://doi.org/10.1016/j.ecohyd.2021.05.002>, 2021.

809 Górska, B., Gromisz, S., Legeżyńska, J., Soltwedel, T., and Włodarska-Kowalczyk, M.: Macro-benthic
810 diversity response to the atlantification of the Arctic Ocean (Fram Strait, 79°N) – A taxonomic and
811 functional trait approach, *Ecol. Indic.*, 144, 109464, <https://doi.org/10.1016/j.ecolind.2022.109464>, 2022.

812 Grant, D. M., Steinsland, K., Cordier, T., Ninnemann, U. S., Ijaz, U. Z., Dahle, H., De Schepper, S., and
813 Ray, J. L.: Sedimentary ancient DNA sequences reveal marine ecosystem shifts and indicator taxa for
814 glacial-interglacial sea ice conditions, *Quat. Sci. Rev.*, 339, 108619,
815 <https://doi.org/10.1016/j.quascirev.2024.108619>, 2024.

816 Guillou, L., Bachar, D., Audic, S., Bass, D., Berney, C., Bittner, L., Boutte, C., Burgaud, G., de Vargas, C.,
817 Decelle, J., del Campo, J., Dolan, J. R., Dunthorn, M., Edvardsen, B., Holzmann, M., Kooistra, W. H. C.
818 F., Lara, E., Le Bescot, N., Logares, R., Mahé, F., Massana, R., Montresor, M., Morard, R., Not, F.,
819 Pawlowski, J., Probert, I., Sauvadet, A. L., Siano, R., Stoeck, T., Vaultot, D., Zimmermann, P., and Christen,
820 R.: The Protist Ribosomal Reference database (PR2): a catalog of unicellular eukaryote Small Sub-Unit
821 rRNA sequences with curated taxonomy, *Nucleic Acids Res.*, 41, D597-D604,
822 <https://doi.org/10.1093/nar/gks1160>, 2012.

823 Hallegraeff, G. M.: Ocean Climate Change, Phytoplankton Community Responses, and Harmful Algal
824 Blooms: A Formidable Predictive Challenge, *J. Phycol.*, 46, 220-235, <https://doi.org/10.1111/j.1529-8817.2010.00815.x>, 2010.

826 Harðardóttir, S., Haile, J. S., Ray, J. L., Limoges, A., Van Nieuwenhove, N., Lalande, C., Grondin, P.,
827 Jackson, R., Skaar, K. S., Heikkilä, M., Berge, J., Lundholm, N., Massé, G., Rysgaard, S., Seidenkrantz,
828 M., De Schepper, S., Lorenzen, E. D., Lovejoy, C., and Ribeiro, S.: Millennial-scale variations in Arctic sea
829 ice are recorded in sedimentary ancient DNA of the microalga *Polarella glacialis*, *Commun. Earth Environ.*,
830 5, <https://doi.org/10.1038/s43247-023-01179-5>, 2024.

831 Hartikainen, H., Ashford, O. S., Berney, C., Okamura, B., Feist, S. W., Baker-Austin, C., Stentiford, G. D.,
832 and Bass, D.: Lineage-specific molecular probing reveals novel diversity and ecological partitioning of
833 haplosporidians, *ISME J.*, 8, 177-186, <https://doi.org/10.1038/ismej.2013.136>, 2014.

834 Heaton, T. J., Köhler, P., Butzin, M., Bard, E., Reimer, R. W., Austin, W. E. N., Bronk Ramsey, C., Grootes,
835 P. M., Hughen, K. A., Kromer, B., Reimer, P. J., Adkins, J., Burke, A., Cook, M. S., Olsen, J., and Skinner,
836 L. C.: Marine20—The Marine Radiocarbon Age Calibration Curve (0–55,000 cal BP), *Radiocarb.*, 62, 779-
837 820, <https://doi.org/10.1017/rdc.2020.68>, 2020.

838 Hop, H., Wold, A., Vihtakari, M., Daase, M., Kwasniewski, S., Gluchowska, M., Lischka, S., Buchholz, F.,
839 and Falk-Petersen, S.: Zooplankton in Kongsfjorden (1996–2016) in Relation to Climate Change, in: *The*
840 *Ecosystem of Kongsfjorden, Svalbard, Advances in Polar Ecology*, 229-300, [https://doi.org/10.1007/978-](https://doi.org/10.1007/978-3-319-46425-1_7)
841 [3-319-46425-1_7](https://doi.org/10.1007/978-3-319-46425-1_7), 2019.

842 Hopkins, T. S.: The GIN Sea: A synthesis of its physical oceanography and literature review 1972–1985,
843 *EARTH-SCI REV.* 30, 175-318, [https://doi.org/10.1016/0012-8252\(91\)90001-V](https://doi.org/10.1016/0012-8252(91)90001-V), 1991.

844 Hoppe, C. J. M., Wolf, K. K. E., Schuback, N., Tortell, P. D., and Rost, B.: Compensation of ocean
845 acidification effects in Arctic phytoplankton assemblages, *Nat. Clim. Change*, 8, 529-533,
846 <https://doi.org/10.1038/s41558-018-0142-9>, 2018.

847 Ibarbalz, F. M., Henry, N., Brandao, M. C., Martini, S., Busseni, G., Byrne, H., Coelho, L. P., Endo, H.,
848 Gasol, J. M., Gregory, A. C., Mahe, F., Rigonato, J., Royo-Llonch, M., Salazar, G., Sanz-Saez, I., Scalco,
849 E., Soviadan, D., Zayed, A. A., Zingone, A., Labadie, K., Ferland, J., Marec, C., Kandels, S., Picheral, M.,
850 Dimier, C., Poulain, J., Pisarev, S., Carmichael, M., Pesant, S., Tara Oceans, C., Babin, M., Boss, E.,
851 Iudicone, D., Jaillon, O., Acinas, S. G., Ogata, H., Pelletier, E., Stemmann, L., Sullivan, M. B., Sunagawa,
852 S., Bopp, L., de Vargas, C., Karp-Boss, L., Wincker, P., Lombard, F., Bowler, C., and Zinger, L.: Global
853 Trends in Marine Plankton Diversity across Kingdoms of Life, *Cell*, 179, 1084-1097 e1021,
854 <https://doi.org/10.1016/j.cell.2019.10.008>, 2019.

855 IPCC: Climate Change 2022 – Impacts, Adaptation and Vulnerability: Working Group II Contribution to
856 the Sixth Assessment Report of the Intergovernmental Panel on Climate Change, Cambridge University
857 Press, Cambridge, <https://doi.org/10.1017/9781009325844>, 2023.

858 Irwin, N. A. T., Tikhonenkov, D. V., Hehenberger, E., Mylnikov, A. P., Burki, F., and Keeling, P. J.:
859 Phylogenomics supports the monophyly of the Cercozoa, *Mol. Phylogenet. Evol.*, 130, 416-423,
860 <https://doi.org/10.1016/j.ympev.2018.09.004>, 2019.

861 Jo, T. S., Murakami, H., and Nakadai, R.: Spatial dispersal of environmental DNA particles in lentic and
862 marine ecosystems: An overview and synthesis, *Ecol. Indic.*, 174, 113469,
863 <https://doi.org/10.1016/j.ecolind.2025.113469>, 2025.

864 Kassambara, A.: Ggpubr: 'ggplot2' based publication ready plots,
865 <https://doi.org/10.32614/CRAN.package.ggplot2>, 2018.

866 Kolde, R.: pheatmap: Pretty Heatmaps, <https://doi.org/10.32614/CRAN.package.pheatmap>, 2025.

867 Kruskal, W. H. and Wallis, W. A.: Use of ranks in one-criterion variance analysis, *J. Am. Stat. Assoc.*, 47,
868 583-621, <https://doi.org/10.1080/01621459.1952.10483441>, 1952.

869 Kubiszyn, A. M. and Wiktor, J. M.: The Gymnodinium and Gyrodinium (Dinoflagellata: Gymnodiniaceae)
870 of the West Spitsbergen waters (1999–2010): biodiversity and morphological description of unidentified
871 species, *Polar Biol.*, 39, 1739-1747, <https://doi.org/10.1007/s00300-015-1764-2>, 2016.

872 Kühn, S., Medlin, L., and Eller, G.: Phylogenetic position of the parasitoid nanoflagellate *Pirsonia* inferred
873 from nuclear-encoded small subunit ribosomal DNA and a description of *Pseudopirsonia* n. gen. and
874 *Pseudopirsonia mucosa* (Drebes) comb. nov, *Protist*, 155, 143-156,
875 <https://doi.org/10.1078/143446104774199556>, 2004.

876 Labarre, A., Lopez-Escardo, D., Latorre, F., Leonard, G., Bucchini, F., Obiol, A., Cruaud, C., Sieracki, M.
877 E., Jaillon, O., Wincker, P., Vandepoele, K., Logares, R., and Massana, R.: Comparative genomics reveals
878 new functional insights in uncultured MAST species, *ISME J.*, 15, 1767-1781,
879 <https://doi.org/10.1038/s41396-020-00885-8>, 2021.

880 Łącka, M., Zajączkowski, M., Forwick, M., and Szczuciński, W.: Late Weichselian and Holocene
881 palaeoceanography of Storfjordrenna, southern Svalbard, *Clim. Past.*, 11, 587-603,
882 <https://doi.org/10.5194/cp-11-587-2015>, 2015.

883 Łącka, M., Cao, M., Rosell-Melé, A., Pawłowska, J., Kucharska, M., Forwick, M., and Zajączkowski, M.:
884 Postglacial paleoceanography of the western Barents Sea: Implications for alkenone-based sea surface
885 temperatures and primary productivity, *Quat. Sci. Rev.*, 224, 105973,
886 <https://doi.org/10.1016/j.quascirev.2019.105973>, 2019.

887 Łącka, M., Michalska, D., Pawłowska, J., Szymanska, N., Szczucinski, W., Forwick, M., and Zajaczkowski,
888 M.: Multiproxy paleoceanographic study from the western Barents Sea reveals dramatic Younger Dryas
889 onset followed by oscillatory warming trend, *Sci. Rep.*, 10, 15667, [https://doi.org/10.1038/s41598-020-](https://doi.org/10.1038/s41598-020-72747-4)
890 [72747-4](https://doi.org/10.1038/s41598-020-72747-4), 2020.

891 Lei, Y., Xu, K., and Choi, J. K.: *Holosticha hamulata* n. sp. and *Holosticha heterofoissneri* Hu and Song,
892 2001, two urostyleid ciliates (protozoa, ciliophora) from intertidal sediments of the yellow sea, *J. Eukaryote*.
893 *Microbiol.*, 52, 310-318, <https://doi.org/10.1111/j.1550-7408.2005.00039.x>, 2005.

894 Lejzerowicz, F., Esling, P., Majewski, W., Szczuciński, W., Decelle, J., Obadia, C., Arbizu, P. M., and
895 Pawłowski, J.: Ancient DNA complements microfossil record in deep-sea subsurface sediments, *Biol Lett*,
896 9, 20130283, 10.1098/rsbl.2013.0283, 2013.

897 Li, X., Li, F., Min, X., Xie, Y., and Zhang, Y.: Embracing eDNA and machine learning for taxonomy-free
898 microorganisms biomonitoring to assess the river ecological status, *Ecol. Indic.*, 155, 110948,
899 <https://doi.org/10.1016/j.ecolind.2023.110948>, 2023.

900 Lin, Y. C., Chin, C. P., Yang, J. W., Chiang, K. P., Hsieh, C. H., Gong, G. C., Shih, C. Y., and Chen, S. Y.:
901 How communities of marine stramenopiles varied with environmental and biological variables in the
902 Subtropical Northwestern Pacific Ocean, *Microbe. Ecol.*, 83, 916-928, [https://doi.org/10.1007/s00248-021-](https://doi.org/10.1007/s00248-021-01788-7)
903 [01788-7](https://doi.org/10.1007/s00248-021-01788-7), 2022.

904 Lindeque, P. K., Parry, H. E., Harmer, R. A., Somerfield, P. J., and Atkinson, A.: Next generation sequencing
905 reveals the hidden diversity of zooplankton assemblages, *PLoS One*, 8, e81327,
906 <https://doi.org/10.1371/journal.pone.0081327>, 2013.

907 Lopez-Garcia, P., Vereshchaka, A., and Moreira, D.: Eukaryotic diversity associated with carbonates and
908 fluid-seawater interface in Lost City hydrothermal field, *Environ. Microbiol.*, 9, 546-554,
909 <https://doi.org/10.1111/j.1462-2920.2006.01158.x>, 2007.

910 Love, M. I., Huber, W., and Anders, S.: Moderated estimation of fold change and dispersion for RNA-seq
911 data with DESeq2, *Genome Biol.*, 15, 550, <https://doi.org/10.1186/s13059-014-0550-8>, 2014.

912 Luddington, I. A., Lovejoy, C., and Kaczmarska, I.: Species-rich meta-communities of the diatom order
913 Thalassiosirales in the Arctic and northern Atlantic Ocean, *J. Plankton Res.*, 38, 781-797,
914 <https://doi.org/10.1093/plankt/fbw030>, 2016.

915 Marinovich Jr, L., Barinov, K. B., and Oleinik, A. E.: The *Astarte* (Bivalvia: Astartidae) that document the
916 earliest opening of Bering Strait, *J. Paleontol.*, 76, 239-245, [https://doi.org/10.1666/0022-](https://doi.org/10.1666/0022-3360(2002)076<0239:TABATD>2.0.CO;2)
917 [3360\(2002\)076<0239:TABATD>2.0.CO;2](https://doi.org/10.1666/0022-3360(2002)076<0239:TABATD>2.0.CO;2), 2002.

918 Martrat, B., Grimalt, J. O., Villanueva, J., van Kreveld, S., and Sarnthein, M.: Climatic dependence of the
919 organic matter contributions in the north eastern Norwegian Sea over the last 15,000 years, *Org. Geochem.*,
920 34, 1057-1070, [https://doi.org/10.1016/s0146-6380\(03\)00084-6](https://doi.org/10.1016/s0146-6380(03)00084-6), 2003.

921 Mylnikov, A. P., Weber, F., Jurgens, K., and Wylezich, C.: *Massisteria marina* has a sister: *Massisteria voersi*
922 sp. nov., a rare species isolated from coastal waters of the Baltic Sea, *Eur. J. Protistol.*, 51, 299-310,
923 <https://doi.org/10.1016/j.ejop.2015.05.002>, 2015.

924 Newbold, L. K., Oliver, A. E., Booth, T., Tiwari, B., DeSantis, T., Maguire, M., Andersen, G., van der Gast,
925 C. J., and Whiteley, A. S.: The response of marine picoplankton to ocean acidification, *Environ. Microbiol.*,
926 14, 2293-2307, <https://doi.org/10.1111/j.1462-2920.2012.02762.x>, 2012.

927 Nguyen, N. L., Pawłowska, J., Szymańska, N., Zajaczkowski, M., Weiner, A. K. M., De Schepper, S., and
928 Pawłowski, J.: Assessing the passive dispersal of benthic foraminifera through environmental DNA,
929 *Limnol. Oceanogr.*, 71, e70294, <https://doi.org/10.1002/lno.70294>, 2026.

930 Nikolaev, S. I., Berney, C., Fahrni, J., Mylnikov, A. P., Aleshin, V. V., Petrov, N. B., and Pawłowski, J.:
931 *Gymnophrys cometa* and *Lecythium* sp. are core Cercozoa: evolutionary implications, *Acta Protozool.*, 42,
932 183-190, 2003.

933 Obiol, A., Del Campo, J., de Vargas, C., Mahe, F., and Massana, R.: How marine are Marine Stramenopiles
934 (MAST)? A cross-system evaluation, *FEMS Microbiol. Ecol.* 100, <https://doi.org/10.1093/femsec/fiae130>,
935 2024.

936 Oksanen, J., Simpson, G., Blanchet, F., Kindt, R., Legendre, P., Minchin, P., O'Hara, R., Solymos, P.,
937 Stevens, M., Szocs, E., Wagner, H., Barbour, M., Bedward, M., Bolker, B., Borcard, D., Borman, T.,
938 Carvalho, G., Chirico, M., De Caceres, M., Durand, S., Evangelista, H., FitzJohn, R., Friendly, M.,
939 Furneaux, B., Hannigan, G., Hill, M., Lahti, L., Martino, C., McGlenn, D., Ouellette, M., Ribeiro Cunha,
940 E., Smith, T., Stier, A., Ter Braak, C., and Weedon, J.: *vegan*: Community Ecology Package,
941 <https://doi.org/10.32614/CRAN.package.vegan>, 2025.

942 Paradis, E. and Schliep, K.: *ape* 5.0: an environment for modern phylogenetics and evolutionary analyses
943 in R, *Bioinform.*, 35, 526-528, <https://doi.org/10.1093/bioinformatics/bty633>, 2019.

944 Paulson, J. N., Stine, O. C., Bravo, H. C., and Pop, M.: Differential abundance analysis for microbial
945 marker-gene surveys, *Nat. Methods*, 10, 1200-1202, <https://doi.org/10.1038/nmeth.2658>, 2013.

946 Pawłowska, J., Łącka, M., Kucharska, M., Pawłowski, J., and Zajaczkowski, M.: Multiproxy evidence of
947 the Neoglacial expansion of Atlantic Water to eastern Svalbard, *Clim. Past.*, 16, 487-501,
948 <https://doi.org/10.5194/cp-16-487-2020>, 2020.

949 Pawłowska, J., Lejzerowicz, F., Esling, P., Szczuciński, W., Zajaczkowski, M., and Pawłowski, J.: Ancient
950 DNA sheds new light on the Svalbard foraminiferal fossil record of the last millennium, *Geobiology*, 12,
951 277-288, <https://doi.org/10.1111/gbi.12087>, 2014.

952 Perret-Gentil, L. A., Cordonier, A., Straub, F., Iseli, J., Esling, P., and Pawłowski, J.: Taxonomy-free
953 molecular diatom index for high-throughput eDNA biomonitoring, *Mol. Ecol. Resour.*, 17, 1231-1242,
954 <https://doi.org/10.1111/1755-0998.12668>, 2017.

955 Perret-Gentil, L. A., Bouchez, A., Cordier, T., Cordonier, A., Guéguen, J., Rimet, F., Vasselon, V., and
956 Pawłowski, J.: Monitoring the ecological status of rivers with diatom eDNA metabarcoding: A comparison

957 of taxonomic markers and analytical approaches for the inference of a molecular diatom index, *Mol. Ecol.*,
958 30, 2959-2968, <https://doi.org/10.1111/mec.15646>Digital, 2021.

959 Petersen, G. H.: Studies on some Arctic and baltic Astarte species (Bivalvia, Mollusca), Museum
960 Tusculanum Press 2001.

961 Petz, W., Song, W., and Wilbert, N.: Taxonomy and ecology of the ciliate fauna (Protozoa, Ciliophora) in
962 the endopagial and pelagial of the Weddell Sea, Antarctica, Land Oberösterreich, OÖ Landesmuseum 1995.

963 Polyakov, I. V., Rippeth, T. P., Fer, I., Alkire, M. B., Baumann, T. M., Carmack, E. C., Ingvaldsen, R.,
964 Ivanov, V. V., Janout, M., Lind, S., Padman, L., Pnyushkov, A. V., and Rember, R.: Weakening of Cold
965 Halocline Layer Exposes Sea Ice to Oceanic Heat in the Eastern Arctic Ocean, *J. Clim.*, 33, 8107-8123,
966 <https://doi.org/10.1175/JCLI-D-19-0976.1>, 2020.

967 Polyakov, I. V., Pnyushkov, A. V., Alkire, M. B., Ashik, I. M., Baumann, T. M., Carmack, E. C., Goszczko,
968 I., Guthrie, J., Ivanov, V. V., Kanzow, T., Krishfield, R., Kwok, R., Sundfjord, A., Morison, J., Rember, R.,
969 and Yulin, A.: Greater role for Atlantic inflows on sea-ice loss in the Eurasian Basin of the Arctic Ocean,
970 *Science*, 356, 285-291, <https://doi.org/10.1126/science.aai8204>, 2017.

971 Ribeiro, C. G., Lopes dos Santos, A., Trefault, N., Marie, D., Lovejoy, C., and Vaultot, D.: Arctic
972 phytoplankton microdiversity across the marginal ice zone: Subspecies vulnerability to sea-ice loss, *Elem.*
973 *Sci. Anth.*, 12, <https://doi.org/10.1525/elementa.2023.00109>, 2024.

974 Rintala, J. M., Hällfors, H., Hällfors, S., Hällfors, G., Majaneva, M., and Blomster, J.: *Heterocapsa* *Arctica*
975 *Subsp. Frigida* *Subsp. Nov.* (Peridinales, Dinophyceae)-Description of a New Dinoflagellate and Its
976 Occurrence in the Baltic Sea1, *J. Phycol.*, 46, 751-762, <https://doi.org/10.1111/j.1529-8817.2010.00868.x>,
977 2010.

978 Risebrobakken, B., Moros, M., Ivanova, E. V., Chistyakova, N., and Rosenberg, R.: Climate and
979 oceanographic variability in the SW Barents Sea during the Holocene, *Holocene*, 20, 609-621,
980 <https://doi.org/10.1177/0959683609356586>, 2010.

981 Roberts, D. W.: Statistical analysis of multidimensional fuzzy set ordinations, *Ecol.*, 89, 1246-1260,
982 <https://doi.org/10.1890/07-0136.1>, 2008.

983 Rohart, F., Gautier, B., Singh, A., and Lê Cao, K.: mixOmics: An R package for 'omics feature selection
984 and multiple data integration, *PLoS Comput. Biol.*, 13, e1005752,
985 <https://doi.org/10.1371/journal.pcbi.1005752>, 2017.

986 Rueckert, S., Wakeman, K. C., Jenke-Kodama, H., and Leander, B. S.: Molecular systematics of marine
987 gregarine apicomplexans from Pacific tunicates, with descriptions of five novel species of Lankesteria, *Int.*
988 *J. Syst. Evol. Microbiol.*, 65, 2598-2614, <https://doi.org/10.1099/ijs.0.000300>, 2015.

989 Schweikert, M. and Schnepf, E.: Light and electron microscopical observations on *Pirsonia punctigerae*
990 spec. nov., a nanoflagellate feeding on the marine centric diatom *Thalassiosira punctigera*, *Eur. J. Protistol.*,
991 33, 168-177, [https://doi.org/10.1016/S0932-4739\(97\)80033-8](https://doi.org/10.1016/S0932-4739(97)80033-8), 1997.

992 Sinniger, F., Pawlowski, J., Harii, S., Gooday, A. J., Yamamoto, H., Chevaldonné, P., Cedhagen, T.,
993 Carvalho, G., and Creer, S.: Worldwide Analysis of Sedimentary DNA Reveals Major Gaps in Taxonomic
994 Knowledge of Deep-Sea Benthos, *Front. Mar. Sci.*, 3, 10.3389/fmars.2016.00092, 2016.

995 Skogseth, R., Olivier, L., Nilsen, F., Falck, E., Fraser, N., Tverberg, V., Ledang, A. B., Vader, A., Jonassen,
996 M. O., and Søreide, J.: Variability and decadal trends in the Isfjorden (Svalbard) ocean climate and
997 circulation—An indicator for climate change in the European Arctic, *Prog. Oceanogr.*, 187, 102394,
998 <https://doi.org/10.1016/j.pocean.2020.102394>, 2020.

999 Stoecker, D. K. and Lavrentyev, P. J.: Mixotrophic Plankton in the Polar Seas: A Pan-Arctic Review, *Front.*
1000 *Mar. Sci.*, 5, <https://doi.org/10.3389/fmars.2018.00292>, 2018.

1001 Sundfjord, A., Albretsen, J., Kasajima, Y., Skogseth, R., Kohler, J., Nuth, C., Skarøhamar, J., Cottier, F.,
1002 Nilsen, F., and Asplin, L.: Effects of glacier runoff and wind on surface layer dynamics and Atlantic Water
1003 exchange in Kongsfjorden, Svalbard; a model study, *Estuar. Coast. Shelf Sci.*, 187, 260-272,
1004 <https://doi.org/10.1016/j.ecss.2017.01.015>, 2017.

1005 Team, R. C.: R: A Language and Environment for Statistical Computing [code], 2025.

1006 Telesiński, M., Kucharska, M., Łacka, M., and Zajączkowski, M.: A late response of the sea-ice cover to
1007 Neoglacial cooling in the western Barents Sea, Holocene, 34, 1088-1096,
1008 <https://doi.org/10.1177/09596836241247305>, 2024.

1009 Telesiński, M. M., Przytarska, J. E., Sternal, B., Forwick, M., Szczuciński, W., Łacka, M., and
1010 Zajączkowski, M.: Palaeoceanographic evolution of the SW Svalbard shelf over the last 14 000 years,
1011 *Boreas*, 47, 410-422, <https://doi.org/10.1111/bor.12282Digital>, 2018.

1012 Thomsen, H. A. and Østergaard, J. B.: Acanthoecid choanoflagellates from the Atlantic Arctic Region— a
1013 baseline study, *Heliyon*, 3, <https://doi.org/10.1016/j.heliyon.2017.e00345>, 2017.

1014 Tillmann, U., Wietkamp, S., Gottschling, M., and Hoppenrath, M.: *Prorocentrum pervagatum* sp. nov.
1015 (*Prorocentrales*, *Dinophyceae*): A new, small, planktonic species with a global distribution, *Phycol. Res.*,
1016 71, 56-71, <https://doi.org/10.1111/pre.12502>, 2022.

1017 Wassmann, P., Duarte, C. M., Agustí, S., and Sejr, M. K.: Footprints of climate change in the Arctic marine
1018 ecosystem, *Globe. Chang. Biol.*, 17, 1235-1249, <https://doi.org/10.1111/j.1365-2486.2010.02311.x>, 2010.

1019 Wei, T. and Simko, V.: R package 'corrplot': Visualization of a Correlation Matrix, 2024.

1020 Wickham, H.: *ggplot2: Elegant Graphics for Data Analysis*, Springer-Verlag New York 2016.

1021 Wickham, H.: *stringr: Simple, Consistent Wrappers for Common String Operations*,
1022 <https://doi.org/10.32614/CRAN.package.stringr>, 2025.

1023 Wilbert, N. and Song, W.: A further study on littoral ciliates (Protozoa, Ciliophora) near King George Island,
1024 Antarctica, with description of a new genus and seven new species, *J. Nat. Hist.*, 42, 979-1012,
1025 <https://doi.org/10.1080/00222930701877540>, 2008.

1026 Wollenburg, J. E., Knies, J., and Mackensen, A.: High-resolution paleoproductivity fluctuations during the
1027 past 24 kyr as indicated by benthic foraminifera in the marginal Arctic Ocean, *Palaeogeogr. Palaeoclimatol.*
1028 *Palaeoecol.*, 204, 209-238, [https://doi.org/10.1016/s0031-0182\(03\)00726-0](https://doi.org/10.1016/s0031-0182(03)00726-0), 2004.

1029 Wu, X., Liu, Y., Weng, Y., Li, L., and Lin, S.: Isolation, identification and toxicity of three strains of
1030 *Heterocapsa* (Dinophyceae) in a harmful event in Fujian, China, *Harmful Algae*, 120, 102355,
1031 <https://doi.org/10.1016/j.hal.2022.102355>, 2022.

1032 Xu, D., Song, W., and Hu, X.: Morphology of *Cyclotrichium taniguchii* sp. nov. and *C. cyclokaryon* with
1033 establishment of a new genus, *Dicyclotrichium* gen. nov. (Ciliophora: Haptorida), *J. Mar. Biol. Assoc. UK*,
1034 85, 787-794, <https://doi.org/10.1017/S0025315405011719>, 2005.

1035 Zajączkowski, M.: Sediment supply and fluxes in glacial and outwash fjords, Kongsfjorden and
1036 Adventfjorden, Svalbard, *Pol. Polar Res.*, 29, 59-72, 2008.

1037 Zimmermann, H. H., Stoof-Leichsenring, K. R., Kruse, S., Nürnberg, D., Tiedemann, R., and Herzschuh,
1038 U.: Sedimentary Ancient DNA From the Subarctic North Pacific: How Sea Ice, Salinity, and Insolation
1039 Dynamics Have Shaped Diatom Composition and Richness Over the Past 20,000 Years, *Paleoceanogr.*
1040 *Paleoclimatol.* 36, <https://doi.org/10.1029/2020pa004091>, 2021.

1041 Zimmermann, H. H., Stoof-Leichsenring, K. R., Dinkel, V., Harms, L., Schulte, L., Hutt, M. T., Nürnberg,
1042 D., Tiedemann, R., and Herzschuh, U.: Marine ecosystem shifts with deglacial sea-ice loss inferred from
1043 ancient DNA shotgun sequencing, *Nat. Commun.*, 14, 1650, <https://doi.org/10.1038/s41467-023-36845-x>,
1044 2023.

1045